JBC RESEARCH ARTICLE

Cingulin binds to the ZU5 domain of scaffolding protein ZO-1 to promote its extended conformation, stabilization, and tight junction accumulation

Received for publication, October 15, 2021, and in revised form, February 21, 2022 Published, Papers in Press, March 5, 2022,
https://doi.org/10.1016/j.jbc.2022.101797

Ekaterina Vasileva[1,‡], Domenica Spadaro[1,‡], Florian Rouaud[1,‡], Jonathan M. King[2,3], Arielle Flinois[1], Jimit Shah[1], Sophie Sluysmans[1], Isabelle Méan[1], Lionel Jond[1], Jerrold R. Turner[2], and Sandra Citi[1,*]

From the [1]Department of Cell Biology, Faculty of Sciences, University of Geneva, Geneva, Switzerland; [2]Laboratory of Mucosal Barrier Pathobiology, Department of Pathology, Brigham and Women's Hospital and Harvard Medical School, Boston, Massachusetts, USA; [3]Trinity University, Biology Department, San Antonio, Texas, USA

Edited by Enrique De La Cruz

Zonula occludens-1 (ZO-1), the major scaffolding protein of tight junctions (TJs), recruits the cytoskeleton-associated proteins cingulin (CGN) and paracingulin (CGNL1) to TJs by binding to their N-terminal ZO-1 interaction motif. The conformation of ZO-1 can be either folded or extended, depending on cytoskeletal tension and intramolecular and intermolecular interactions, and only ZO-1 in the extended conformation recruits the transcription factor DbpA to TJs. However, the sequences of ZO-1 that interact with CGN and CGNL1 and the role of TJ proteins in ZO-1 TJ assembly are not known. Here, we used glutathione-*S*-transferase pulldowns and immunofluorescence microscopy to show that CGN and CGNL1 bind to the C-terminal ZU5 domain of ZO-1 and that this domain is required for CGN and CGNL1 recruitment to TJs and to phase-separated ZO-1 condensates in cells. We show that KO of CGN, but not CGNL1, results in decreased accumulation of ZO-1 at TJs. Furthermore, ZO-1 lacking the ZU5 domain showed decreased accumulation at TJs, was detectable along lateral contacts, had a higher mobile fraction than full-length ZO-1 by fluorescence recovery after photobleaching analysis, and had a folded conformation, as determined by structured illumination microscopy of its N-terminal and C-terminal ends. The CGN–ZU5 interaction promotes the extended conformation of ZO-1, since binding of the CGN–ZO-1 interaction motif region to ZO-1 resulted in its interaction with DbpA in cells and in vitro. Together, these results show that binding of CGN to the ZU5 domain of ZO-1 promotes ZO-1 stabilization and accumulation at TJs by promoting its extended conformation.

Tight junctions (TJs) are essential to compartmentalize tissues and maintain body homeostasis (1–3) and consist of transmembrane proteins and a cytoplasmic plaque of scaffolding and adaptor proteins, including ZO proteins (ZO-1, ZO-2, and ZO-3) (4–6), cingulin (CGN), and paracingulin (CGNL1, JACOP [junction-associated-coiled-coil protein]), which connect membrane proteins to the cytoskeleton (reviewed in Refs. (7–9)).

CGN is exclusively localized at TJs (10), where it is recruited by ZO-1 (11). CGNL1 is localized both at TJs and at cadherin-based circumferential adherens junctions (AJs) (*zonulae adhaerentes* [ZA]) (12), where it is recruited by ZO-1 and pleckstrin homology domain–containing family A member 7 (PLEKHA7), respectively (13). CGN and CGNL1 are homodimers that comprise globular head, coiled-coil rod, and globular tail domains and interact with ZO proteins, guanine nucleotide exchange factors (GEFs), and GTPase-activating proteins, as well as cytoskeletal proteins, such as actin, myosin, and microtubules (8, 10, 12, 14–19). Although binding of CGN and CGNL1 to C-terminal ZO-1 sequences is suggested by yeast-2-hybrid screens (20) and BioID experiments (21), the precise sequences of ZO-1 that bind to CGN and CGNL1 have not been mapped.

Despite being the first TJ protein discovered, the mechanisms by which ZO-1 assembles at TJs and interacts with other proteins to regulate junctional structure remain poorly understood. Studies using early *Xenopus* embryos have shown that fusion of ZO-1-containing vesicles with basolateral membranes is followed by sorting of ZO-1 to CGN-containing apical TJs (22). Fluorescence recovery after photobleaching (FRAP) experiments demonstrate that the TJ structure is highly dynamic and that junction-associated ZO-1 exchanges with a mobile cytoplasmic ZO-1 pool (23). Within junctions, ZO-1 can be either extended or folded, depending on actomyosin tension and heterodimerization with ZO-2 (24). Cytoplasmic ZO-1 can assume a liquid–liquid phase state, and ZO-1 extension triggers a phase transition that drives TJ assembly (25). Separate work has found that the C-terminal half of ZO-1 is required for junctional mechanosensitivity (26) and for myosin light-chain kinase–dependent regulation of ZO-1 FRAP behavior and barrier function (27). As a whole, these data suggest that the C-terminal region of ZO-1 mediates interactions that modulate ZO-1 dynamics, conformation, liquid–liquid phase separation and TJ assembly, and barrier regulation (28).

Here, we show that CGN and CGNL1 bind to the C-terminal ZU5 domain of ZO-1 and we test the hypothesis that this

‡ These authors contributed equally to this work.
* For correspondence: Sandra Citi, Sandra.Citi@unige.ch.

interaction induces ZO-1 extended conformation, and its assembly and stabilization at TJs. Our results demonstrate that ZU5 domain–mediated interaction with CGN promotes the ZO-1 extended conformation and is required for stabilization and efficient accumulation of ZO-1 and ZO-3, but not ZO-2, at epithelial TJs.

Results

CGN and CGNL1 bind to the ZU5 domain of ZO-1

To map the region of ZO-1 that binds to CGN, we expressed ZO-1 prey constructs comprised of different C-terminal fragments of ZO-1 as GFP fusion proteins (scheme of ZO-1 prey constructs in Fig. 1*A*, prey normalizations in Fig. 1, *B* and *C*). We tested how these preys interact with a bait consisting of glutathione-*S*-transferase (GST) fused to a small N-terminal CGN fragment (CGN(1-70)) that contains the ZO-1 interaction motif (ZIM), which mediates CGN binding to ZO-1 (29) (bait scheme in Fig. 1*A*). Only ZO-1 preys that contained the C-terminal ZU5 domain (ZU5 = 1634–1748) interacted by GST pulldown with the ZIM-containing (GST–CGN(1-70)) bait (Fig. 1*D*, GST negative control in Fig. 1*E*). The binding of the ZIM-containing fragment to a 129-residue ZO-1 C-terminal fragment (Cter = 1619–1748) that includes

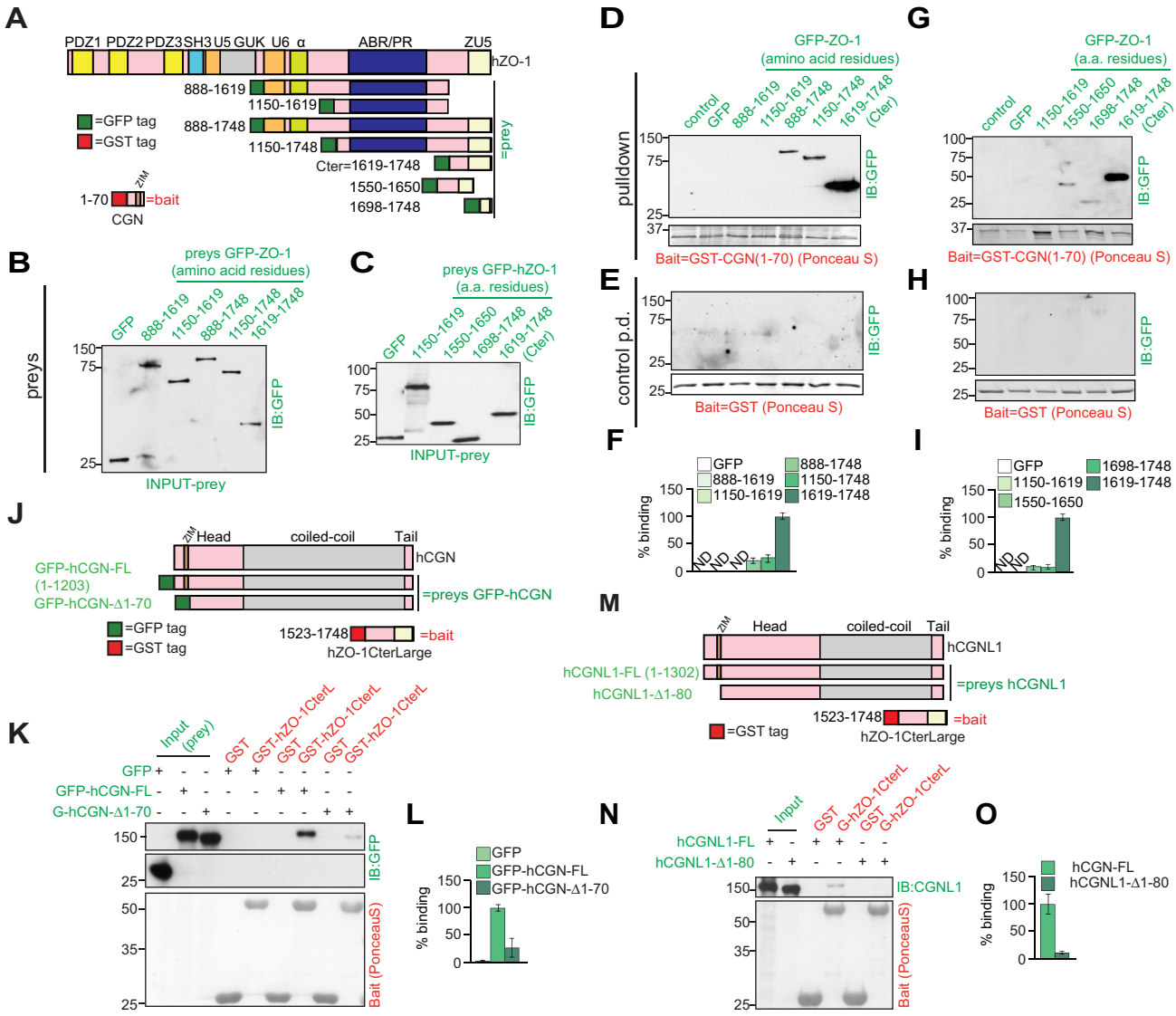

Figure 1. Cingulin (CGN) and paracingulin (CGNL1) bind to the ZU5 domain of ZO-1. *A*, schematic representation of ZO-1 (structural domains are denoted by *colors* and annotated), GFP-tagged ZO-1 prey constructs, and GST-tagged CGN bait construct used for pulldowns (*D–G*). *B–H*, IB analysis, using anti-GFP antibodies, of normalized preys (*B* and *C*), and of GST pulldowns using either GST-CGN (1–70 amino acids) (*D* and *G*) or GST (*E* and *H*) as baits, and GFP-tagged fragments of ZO-1 as preys. *F* and *I*, densitometric quantification of binding of indicated preys to the GST-CGN (1–70 amino acids) fragment. Preys in (*B*) refer to pulldowns shown in (*C–F*) (large ZO-1 fragments). Preys in (*C*) refer to pulldowns shown in (*G–I*) (Cter/ZU5 domain and its fragments). Numbers indicate migration of prestained size markers. Baits are indicated in *red*, and preys are indicated in *green text*. Ponceau S-stained baits are shown below the IB. GST alone is used as a negative control bait. *J* and *K*, scheme of CGN prey and ZO-1 bait constructs (*J*) used in pulldowns (*K*). *K*, IB analysis, using anti-GFP antibodies, of GST pulldowns using GST-hZO-1-CterLarge (CterL, 1523–1748) as a bait and either GFP or GFP-tagged CGN constructs as preys. *L*, densitometric quantification of binding of CGN preys to the GST-hZO-1-CterL bait (IB in [*K*]). *M–O*, scheme of CGNL1 prey and ZO-1 bait constructs (*M*) and IB analysis (*N*) and densitometric quantification (*O*) of IB using anti-CGNL1 antibodies, of GST pulldowns using GST-hZO-1CterL as a bait and hCGNL1 constructs as preys.

the ZU5 sequence was greater than fourfold stronger than to larger fragments (Fig. 1*D* and quantification in Fig. 1*F*). Fragmenting the C-terminal ZU5-containing sequence decreased the interaction with the CGN(1–70) bait (Fig. 1, *G* and *H*, quantification in Fig. 1*I*), indicating that the integrity of the ZU5 domain is required for high-affinity binding of ZO-1 to CGN. Moreover, a bait comprising GST fused to the C-terminal 225 residues of ZO-1 (ZO-1-CterLarge, 1523–1748), which also contains the complete ZU5 sequence, interacted strongly with a full-length (FL) CGN prey, but only very weakly with a deletion of CGN lacking the first 70 residues, which contain the ZIM region (scheme in Fig. 1*J*, pulldown and quantification in Fig. 1, *K* and *L*). This indicates that the ZU5 domain binds to the same region of CGN as FL ZO-1 (29), i.e. it only binds to the N terminus of CGN. Similarly, FL CGNL1 interacted with the ZU5-containing ZO-1-CterLarge bait, but CGNL1 lacking the ZIM region did not (scheme in Fig. 1*M*, pulldown and quantification in Fig. 1, *N* and *O*). These results demonstrate that both CGN and CGNL1 interact with the ZU5 domain of ZO-1 through their ZIM-containing N-terminal sequences.

The ZU5 domain of ZO-1 is required for CGN and CGNL1 recruitment to TJs and to ZO-1 condensates in cells

ZO-1 recruits CGN and CGNL1 to TJs (11, 13), and ZO-1-KO cells completely lack junctional CGN (*arrowhead* in mixed WT-KO culture, Fig. 2*A*) (11). To assess the physiological relevance of the interaction of the ZU5 domain with CGN and CGNL1, we rescued ZO-1-KO Eph4 cells with WT and mutated constructs of ZO-1 and analyzed the junctional recruitment of CGN and CGNL1. FL ZO-1 efficiently rescued endogenous CGN signal at TJs (*arrow*, Fig. 2*B*). In contrast, a construct of ZO-1 lacking the last 129 residues and thus the ZU5 domain (ZO-1–ΔZU5, 1–1619) was targeted to TJs (*arrow in red channel*, Fig. 2*C*) but failed to rescue CGN junctional labeling (*arrowhead in green channel*, Fig. 2*C*), demonstrating that the ZU5–CGN interaction is required for CGN recruitment to TJs in cells.

CGNL1 is localized both at TJs and at AJs (ZA) (12). In agreement, cells KO for ZO-1 showed a decrease but not a complete loss of CGNL1 junctional labeling (*arrowhead in red channel* in Fig. 2*D*, quantification in Fig. 2*G*, *left graph*) (see also Ref. (13)). Expression of FL ZO-1 in ZO-1-KO cells rescued complete CGNL1 junctional labeling (*arrow*, in Fig. 2*E*; quantification in Fig. 2*G*, *right graph*), whereas expression of C-terminally truncated ZO-1, lacking the ZU5 domain (myc-ZO-1-ΔZU5), failed to rescue complete CGNL1 junctional labeling (*arrowhead* in Fig. 2*F*, quantification in Fig. 2*G*, *right graph*).

Next, we examined the recruitment of CGN and CGNL1 in ZO-1 phase-separated condensates, which are produced when ZO-1 is overexpressed in cells (25). Labeling for both CGN or CGNL1 was colocalized with ZO-1 in condensates generated in Madin–Darby canine kidney (MDCK) cells by overexpression of FL ZO-1 (*arrows*, *top*, and *bottom*, respectively, for CGN and CGNL1; Fig. 2*H*). In contrast, CGN and CGNL1 were not detected in ZO-1 condensates in cells overexpressing a mutant of ZO-1 lacking the ZU5 domain (*arrowheads*, *top*, and *bottom*, respectively, for CGN and CGNL1; Fig. 2*I*).

Together, these results demonstrate that the ZU5 domain of ZO-1 interacts with the ZIM-containing N-terminal regions of both CGN and CGNL1 *in vitro* and in cells, and this interaction is required for the recruitment of CGN and CGNL1 to both TJs and ZO-1 condensates in cells.

CGN but not CGNL1 promotes the efficient accumulation of ZO-1 at TJs

Since the ZU5 domain is involved in intramolecular interactions that we proposed to occur in and stabilize the folded conformation of ZO-1 (24), we wondered whether CGN and CGNL1 could regulate ZO-1 conformation and TJ assembly. To address this question, we generated clonal lines of mouse mammary (Eph4), mouse cortical collecting duct epithelial cell line (mCCD), and dog kidney (MDCK II) epithelial cells with CRISPR–Cas9 KO of either *CGN*, or *CGNL1*, or both (Fig. S1, *A*–*Q*). CGN levels were not altered in CGNL1-KO cells and vice versa, indicating no compensatory upregulation (Fig. S1*R*). Moreover, the levels of expression of several TJ and AJ protein markers, including ZO-1, ZO-2, and ZO-3, E-cadherin, and afadin (Fig. S1*R*), and the proliferation rates of the KO lines (Fig. S1*S*) were similar in WT and KO lines, indicating that the KO of either CGN, CGNL1, or both does not result in dramatic changes either in junctional protein expression or cell growth. However, we noticed that ZO-1 junctional labeling was decreased in all three independent CGN-KO MDCK clonal lines, when compared with WT (*arrowheads*, Fig. S1*G*).

To further examine the role of CGN and CGNL1 in the junctional accumulation of ZO-1, we compared ZO-1 immunofluorescent labeling in cultures of WT cells mixed together with either CGN-KO or CGNL1-KO cells, using either Eph4 (Figs. 3 and S2, *A*, *B*, *H* and *I*), mCCD (Fig. S2, *C*, *D*, *J* and *K*) or MDCK (Figs. S2, *E*, *F*, *L* and *M*) cells, and either PLEKHA7 or occludin as a junctional reference marker protein for quantification. ZO-1 immunofluorescent signal at junctions was reduced in CGN-KO Eph4 (*arrowheads*, Figs. 3*A* and S2*A*, quantifications in Fig. S2*B*), mCCD (*arrowheads*, Fig. S2*C*, quantifications in Fig. S2*D*), and MDCK cells (*arrowhead*, Fig. S2*E*, quantifications in Fig. S2*F*), when compared with neighboring WT cells. In contrast, ZO-1 labeling was similar in WT *versus* CGNL1-KO Eph4 (*arrows*, Figs. 3*B* and S2*J*, quantifications in Fig. S2*K*), mCCD (*arrows*, Fig. S2*H*, quantification in Fig. S2*I*), and MDCK cells (*arrows*, Figs. S1*M* and S2*L*, quantifications in Fig. S2*M*).

The decrease in ZO-1 labeling in CGN-KO cells was observed not only using different cell lines but also using three distinct antibodies against ZO-1 (Fig. S2, *A*, *C*, *H*, and *J*). Furthermore, immunoblot (IB) analysis with different anti-ZO-1 antibodies showed that WT cells and different clonal lines KO for either CGN or CGNL1 have similar levels of expression of both α(+) and α(−) isoforms of ZO-1 (Fig. S2, *G* and *N*). This indicates that decreased ZO-1 accumulation at TJs of CGN-KO cells is not caused by either protein degradation or a selective loss of a specific isoform, or to epitope availability. Together, these observations indicate that the

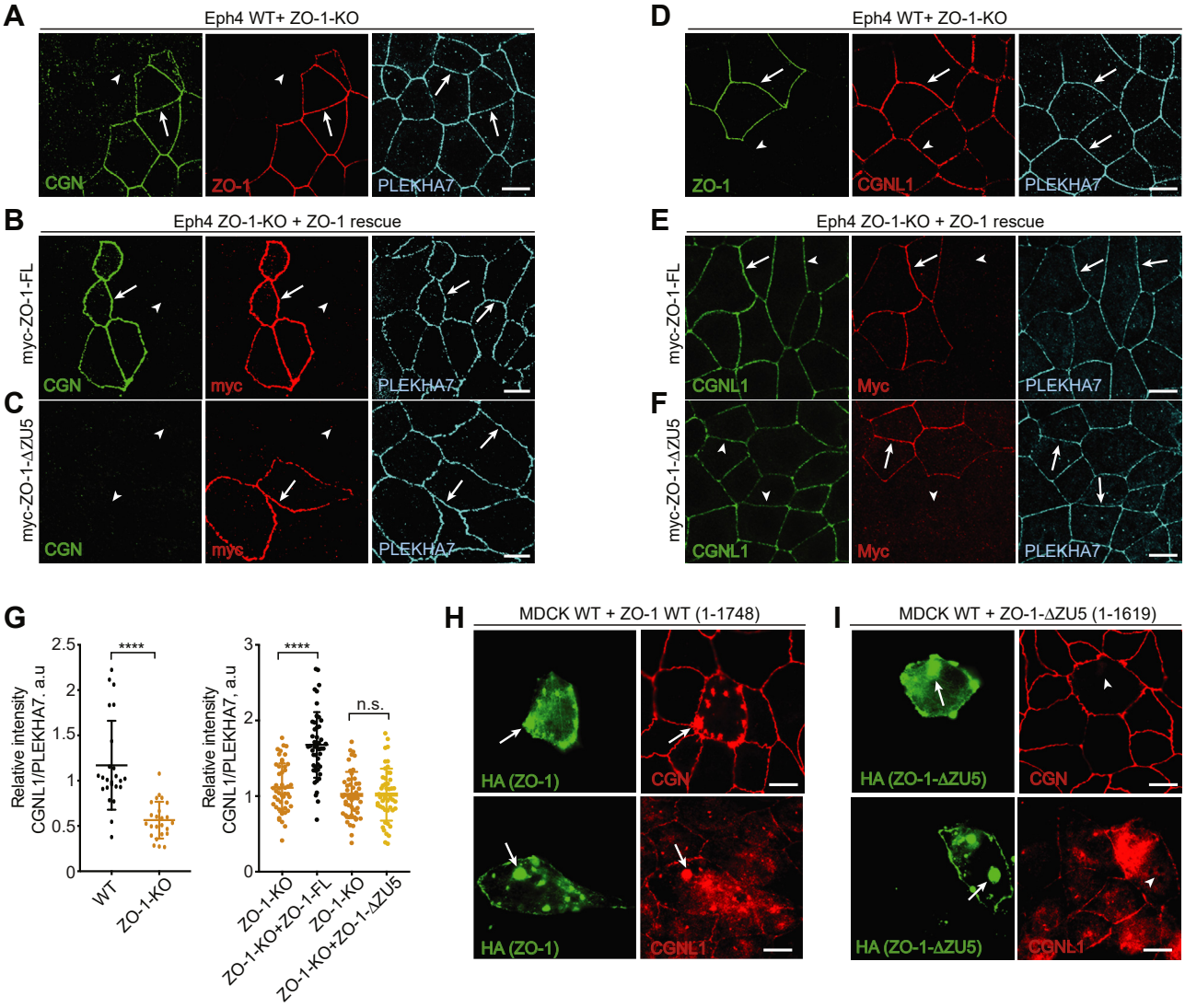

Figure 2. Cingulin (CGN) and paracingulin (CGNL1) are recruited to TJs and to ZO-1 condensates by the ZU5 domain of ZO-1. A–*F*, immunofluorescence (IF) microscopy analysis of the localization of endogenous CGN (*A–C*), CGNL1 (*D–F*), and PLEKHA7 (used as an apical junction marker), and of either endogenous ZO-1 (*A* and *D*) or exogenous myc-tagged ZO-1 rescue constructs (*B–F*) either in mixed WT-ZO-1-KO Eph4 cells (*A* and *D*) or in Eph4 ZO-1-KO cells rescued with either with FL-ZO-1 (*B* and *E*) or with a C-terminal truncation of ZO-1 lacking the ZU5 domain (1–1619) (*C* and *F*) (*red*). *Arrows* and *arrowheads* indicate normal and reduced/undetectable staining, respectively. The scale bars represent 10 μm. *G*, quantification of junctional CGNL1 in mixes of WT-KO cells (*D*) (*left graph*) and in ZO-1-KO cells rescued with either FL or C-terminally truncated ZO-1 (*E* and *F*) (*right graph*). *Dots* show replicates (n = 23), and *bars* represent mean ± SD. One-way ANOVA with post hoc Dunnett's test (****$p < 0.0001$, ns). *H* and *I*, IF microscopy analysis of ZO-1 condensates generated by overexpression of either FL myc-ZO-1-HA (*H*) or myc-ZO-1-ΔZU5-HA (*I*) in WT MDCK cells using antibodies against HA (*green*, to detect exogenous ZO-1) and against either endogenous CGN (*red*, *top panels*) or CGNL1 (*red*, *bottom panels*). The scale bars represent 10 μm.

phenotype of either reduced or normal ZO-1 accumulation at junctions in CGN-KO and CGNL1-KO cells, respectively, is not dependent either on cell type, or antibody reactivity, or isoform expression.

Next, to confirm that the reduction in ZO-1 labeling in CGN-KO cells was specifically caused by the loss of CGN, and not to clone-dependent variations, we rescued the localization of ZO-1 through exogenous CGN expression. FL myc-tagged CGN rescued ZO-1 junctional accumulation (*arrows* in Fig. 3*C*, CGN FL-myc, and quantification in Fig. 3*E*), whereas a mutant of CGN lacking the first 70 amino acid residues, which contain the ZIM, did not localize at junctions and did not rescue ZO-1 junctional labeling (*arrowheads*, Fig. 3*C*, mCGN-Δ1-70-myc, quantification in Fig. 3*E*).

We also asked whether CGN overexpression in the background of WT cells would affect ZO-1 accumulation. Neither the overexpression of FL CGN nor the N-terminally truncated mutant that fails either to bind to ZO-1 or target to TJs resulted in significant changes in ZO-1 junctional labeling (Fig. 3*D*, quantification in Fig. 3*E*), suggesting that in WT cells, ZO-1 junctional pools are already saturated.

The ZU5 domain promotes the stabilization of ZO-1, its accumulation at apical junctions, and its less dynamic FRAP behavior

We next evaluated the contribution of the ZU5 domain to ZO-1 localization at TJs. Exogenous enhanced GFP (eGFP)-

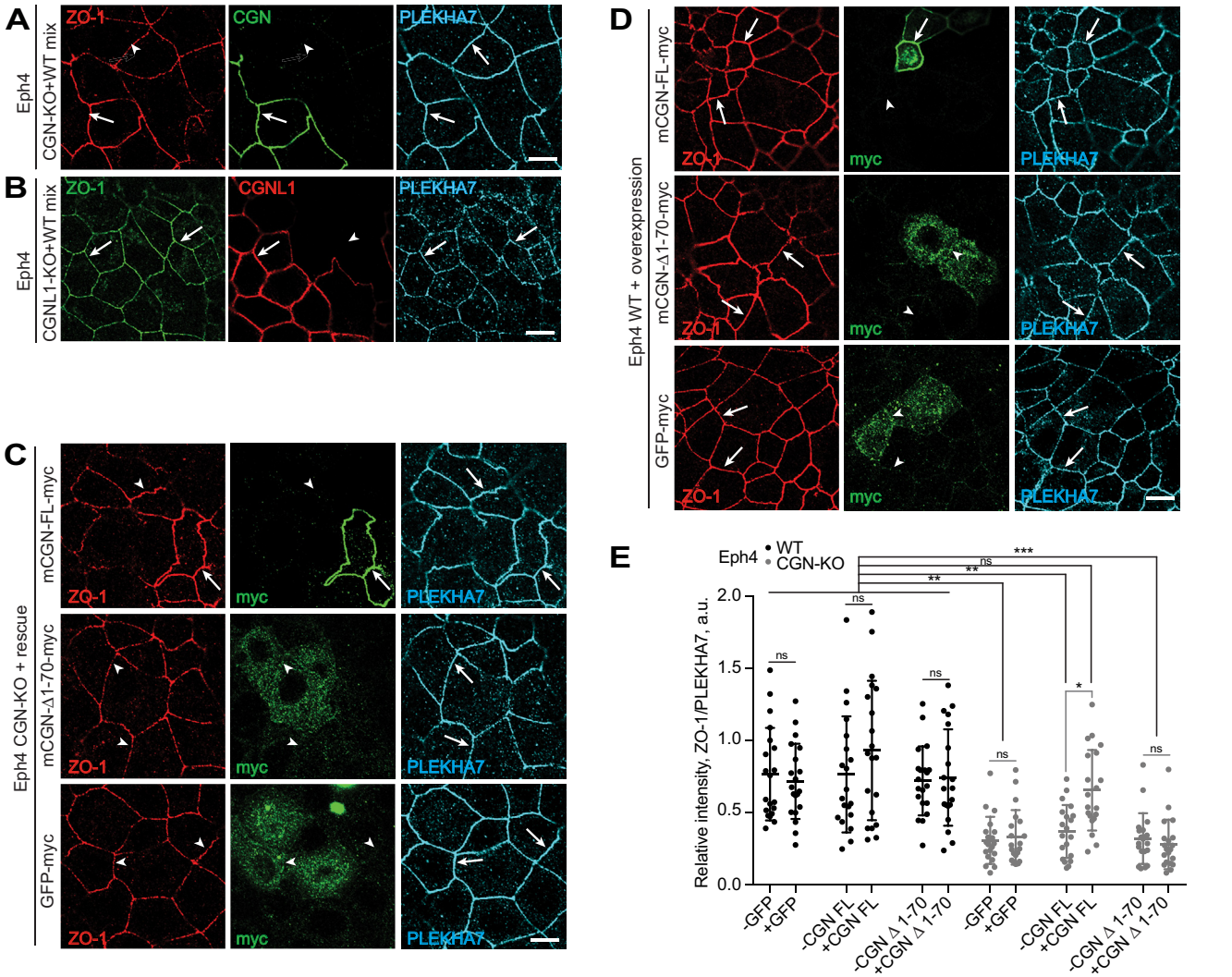

Figure 3. The cingulin (CGN)–ZU5 interaction is required for the efficient accumulation of ZO-1 at TJs. *A–D*, IF microscopy analysis of junctional ZO-1 labeling either in mixed cultures of Eph4 WT cells and cells KO for either CGN (*A*) or paracingulin (CGNL1) (*B*) or in Eph4 CGN-KO cells rescued either with full-length (FL) CGN (CGN-FL-myc) or with an N-terminal truncation of CGN (CGN-Δ1-70-myc) (*C*), or in Eph4 WT cells with overexpression of either FL CGN (CGN-FL-myc) or CGN-Δ1-70-myc, or GFP (negative control) (*D*). PLEKHA7 (*cyan*) was used as a reference junctional marker for quantifications (*E*). *Arrows* and *arrowheads* indicate normal and reduced/undetected junctional staining, respectively. The scale bars represent 10 μm. *E*, quantification of ZO-1 junctional IF signal in either WT or CGN-KO cells after rescue with either GFP-myc or FL or N-terminally truncated CGN constructs. Data are represented as mean ± SD (n = 20). One-way ANOVA with post hoc Dunnett's test (*$p < 0.05$, **$p < 0.01$, and ***$p < 0.001$).

tagged human ZO-1, either FL (eGFP-hZO-1) or lacking the ZU5 domain (eGFP-hZO-1-ΔZU5), was expressed in MDCK cells, and junctional signal intensity was evaluated by confocal immunofluorescence (IF) microscopy (Fig. 4, *A–C*). FL ZO-1 was present at junctional sites and restricted to the apical junctional complex (*white arrow*, Fig. 4*A*), since it was not detectable at lateral contacts (*red arrowhead*, Fig. 4*A*, orthogonal xz section). In contrast, exogenous eGFP-hZO-1-ΔZU5 was detectable both at apical junctions (*white arrow*, Fig. 4*B*) and along lateral contacts (*red arrow*, Fig. 4*B*). Moreover, eGFP-hZO-1-ΔZU5 intensity at apical junctional complexes, relative to E-cadherin, was significantly reduced when compared with FL ZO-1 (Fig. 4*B*, quantification in Fig. 4*C*). These observations suggest that the ZU5 domain is required for efficient ZO-1 recruitment and retention at TJs.

ZO-1 exhibits dynamic behavior, and FRAP studies show that ZO-1 exists in nonexchangeable and exchangeable junction-associated and cytoplasmic pools (23). To study the impact of the ZU5 domain on ZO-1 dynamic behavior, we compared FRAP behavior of FL eGFP-hZO-1 with that of eGFP-hZO-1-ΔZU5. ZU5 deletion significantly accelerated FRAP recovery (Fig. 4, *D* and *F*, representative kymographs in Fig. 4*G*, live imaging in Supporting Movies M1 and M2) and increased mobile fraction (Fig. 4*E*). Together, these results indicate that the ZU5 domain enhances ZO-1 anchoring at the TJs.

Neither CGN nor CGNL1 control ZO-2 TJ assembly, but CGN promotes the accumulation of ZO-3 at TJs

CGN binds not only to ZO-1 but also to ZO-2 and ZO-3 (14). Thus, we asked whether either CGN or CGNL1 KO or double CGN/CGNL1 KO affects the junctional accumulation of ZO-2 and ZO-3, in addition to ZO-1 (Figs. S3, S4, and 5).IF microscopy analysis showed that in the background of either

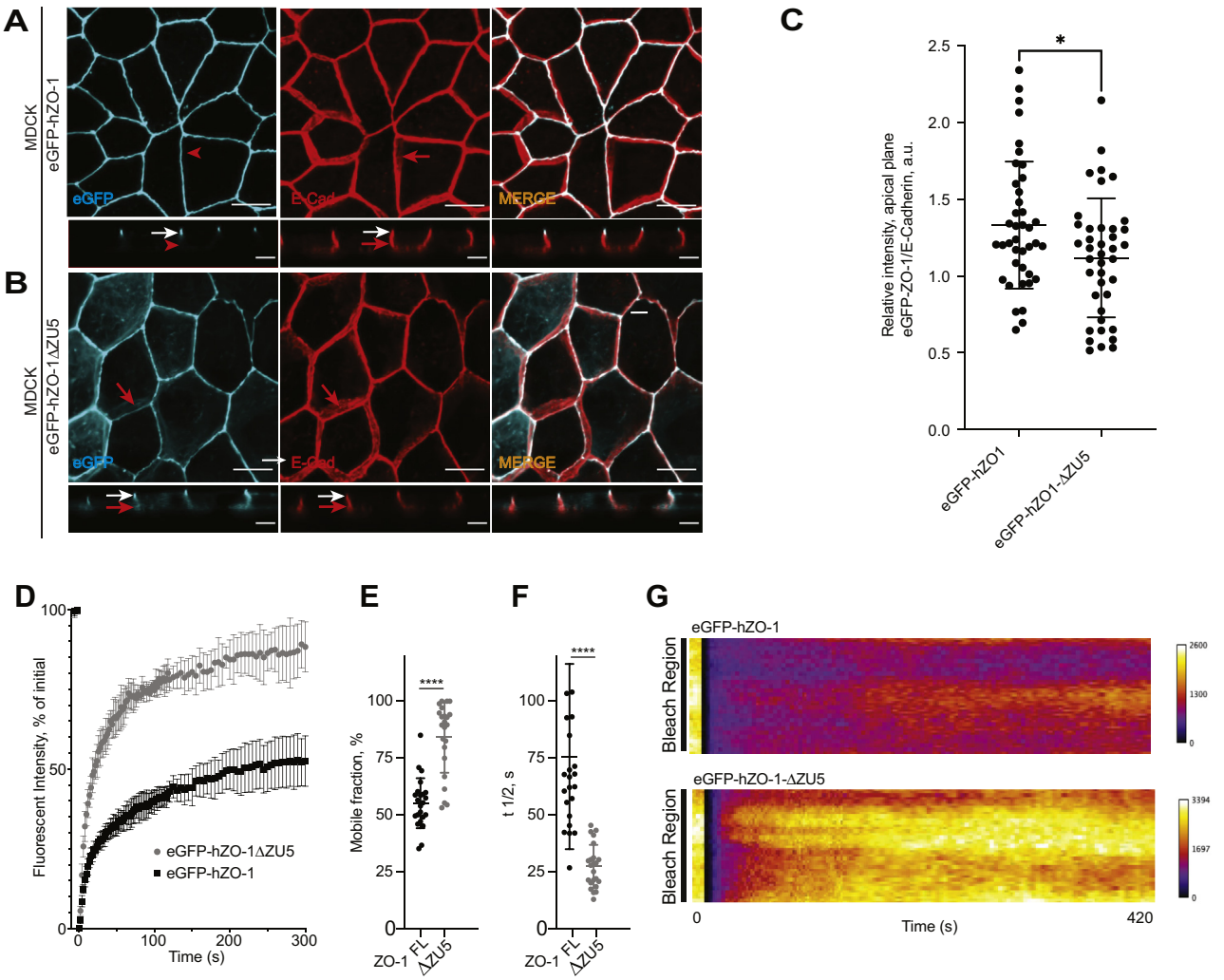

Figure 4. The ZU5 domain of ZO-1 regulates the dynamics and TJ stabilization of ZO-1. *A* and *B*, IF microscopy analysis of exogenous eGFP-tagged ZO-1 (eGFP fluorescence, *cyan*), either full-length (FL) (eGFP-hZO-1) (*A*) or C-terminally truncated (eGFP-hZO-1ΔZU5) (*B*) and E-cadherin (E-Cad, *red*) in fixed WT MDCK cells. The scale bars represent 10 μm. Orthogonal xz images (the scale bar represents 5 μm) are shown below each xy plane. *White arrows* indicate colocalization of ZO-1 and E-Cad at apical junctions, *red arrows* indicate localization/colocalization along lateral contacts, and the *red arrowhead* in (*A*) indicates undetectable signal of FL ZO-1 along lateral regions. *C*, quantification of apical junctional eGFP-hZO-1 signal relative to E-Cad in either FL eGFP-hZO-1-1ΔZU5-expressing cells or eGFP-hZO-1ΔZU5-expressing cells. *Dots* show replicates (n = 40), and bars represent mean ± SD. Statistics: unpaired *t* test (*$p < 0.05$). *D–G*, quantitative FRAP analysis (*D*) of either eGFP-hZO-1 (*black dots*) or eGFP-hZO-1ΔZU5 (*gray dots*) in MDCK cells. *E*, mobile fraction and (*F*) *t* ½ values determined from FRAP curves shown in (*D*). *Dots* in (*E* and *F*) show replicates (n = 21–23), and bars represent mean ± SD. Excluded outliers were identified using ROUT method (Q = 1%). Statistics: unpaired *t* test (****$p < 0.0001$). *G*, representative kymographs of eGFP-tagged ZO-1-full length (*top*) and eGFP-ZO-1ΔZU5 (*bottom*). Related Movies S1 and S2 show live imaging of FRAP of cells expressing either eGFP-ZO-1-FL or eGFP-ZO-1ΔZU5.

Eph4, or mCCD, or MDCK cells, junctional ZO-2 labeling was not affected by KO of either CGN (Fig. S3*A*) or CGNL1 (Fig. S3*B*). IB analysis further indicated that expression of ZO-2 was not significantly affected by the KO of either CGN (Fig. S3*C*) or CGNL1 (Fig. S3*D*). In contrast, ZO-3 junctional labeling was significantly decreased in CGN-KO mCCD and MDCK cells (*arrowheads* in Fig. S4*A*, quantification in Fig. S4*B*) and in double-KO MDCK cells (*arrowhead*, Fig. 5*B*) but not in CGNL1-KO mCCD and MDCK cells (*arrow* in Fig. S4*C*, quantification in Fig. S4*D*). The expression levels of ZO-3 were not affected in either CGN-KO or CGNL1-KO cells (Fig. S4, *E* and *F*). Since ZO-1 forms heterodimers with ZO-3 (30), we asked whether the reduced junctional levels of ZO-3 could be due to reduced ZO-1. To address this question, we overexpressed either FL CGN or FL ZO-1 in the background of CGN-KO cells. Only the expression of CGN resulted in increased accumulation of ZO-3 labeling at junctions (*double arrows*, Fig. S4*G*, quantification in Fig. S4*H*), indicating that reduced junctional ZO-3 in CGN-KO cells depends on CGN and not on ZO-1 levels.

CGN interacts with ZO-3 (14), but the region of ZO-3 that interacts with CGN is not known. By GST pull-down assay, both the C-terminal regions of ZO-1 and ZO-3 interacted with FL CGN, but the >10-fold weaker IB signal indicated that ZO-3 binds to CGN with significantly lower apparent affinity with respect to the ZU5 domain of ZO-1 (Fig. S5*A*). The C-terminal 382 residues of ZO-3 bound to both CGN and CGNL1 (Fig. S5, *B* and *C*), and the ZU5 domain of ZO-1 bound to FL CGN with much higher apparent affinity than FL CGNL1, based on >10-fold stronger IB signal (Fig. S5*C*).

The observation that the KO of CGNL1 has no detectable effect on either ZO-1 or ZO-3 accumulation at TJs (Figs. 3*B*

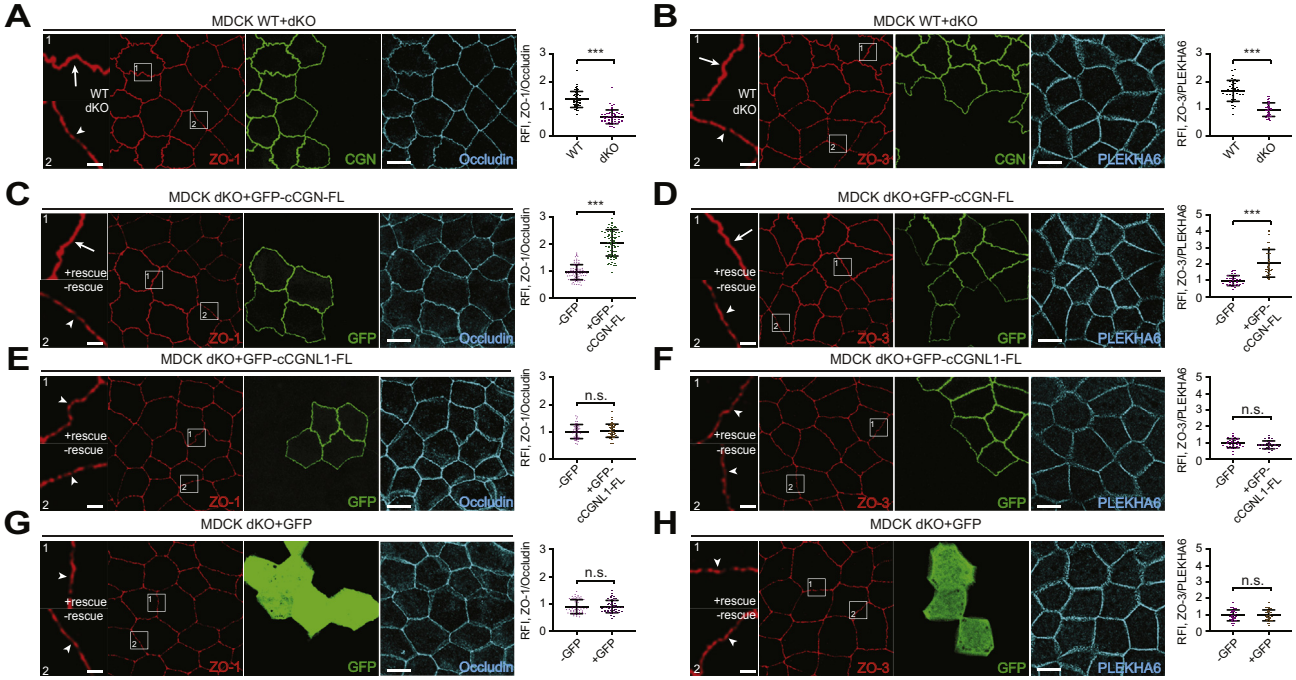

Figure 5. Cingulin (CGN) but not paracingulin (CGNL1) promotes the efficient accumulation of ZO-1 and ZO-3 at tight junctions. *A–H*, IF microscopy analysis and quantification of junctional labeling for endogenous ZO-1 (*A*, *C*, *E*, and *G*) and ZO-3 (*B*, *D*, *F*, and *H*) either in mixes of WT cells and CGN/CGNL1 double-KO (dKO) MDCK cells (*A* and *B*) or in dKO cells overexpressing either full-length GFP-tagged cCGN (*C* and *D*) or full-length GFP-tagged cCGNL1 (*E* and *F*), or GFP (*G* and *H*), cells grown on Transwell filters (pore size of 0.4 μm, polyester). Insets on the *left* of images show high magnification details of areas outlined in *square boxes* (insets; the scale bar represents 100 nm). Endogenous CGN was used to distinguish WT from dKO cells (*A* and *B*), and anti-GFP antibody was used to label exogenous rescue constructs (*C* and *H*). Either occludin (*A*, *C*, *E*, and *G*) or PLEKHA6 (*B*, *D*, *F*, and *H*) was used as reference junctional markers for IF labeling quantifications. *Arrows* and *arrowheads* indicate normal/increased and decreased ZO-1 and ZO-3 junctional labeling, respectively. The scale bars (normal magnification panels) represents 10 μm. Data in plots are represented as mean ± SD. One-way ANOVA with post hoc Dunnett's test (***$p < 0.001$).

and S4, *C* and *D*) could reflect either the low CGNL1 expression in epithelial cells (31), or the partial localization of CGNL1 at TJs (12, 13), or to the relatively weak binding of CGNL1 to ZO-1 ZU5 domain (Fig. S5*C*), or a combination of these mechanisms. To determine if low levels of expression of CGNL1 are involved, we exogenously overexpressed either CGN or CGNL1 in CGN/CGNL1-double-KO cells. IF microscopy showed a reduced junctional accumulation of both ZO-1 (*arrowhead* in magnified inset, Fig. 5*A*) and ZO-3 (*arrowhead* in magnified inset, Fig. 5*B*) in double-KO cells. Importantly, while CGN re-expression in double-KO cells resulted in increased labeling for both ZO-1 (*arrow* in magnified inset, Fig. 5*C*) and ZO-3 (*arrow* in magnified inset, Fig. 5*D*), no rescue of either ZO-1 or ZO-3 labeling was observed in cells over-expressing either FL CGNL1 (*arrowheads* in magnified insets, Fig. 5, *E* and *F*) or GFP alone (*arrowheads* in magnified insets, Fig. 5, *G* and *H*). These results indicate that CGNL1, even when overexpressed, does not promote TJ accumulation of ZO-1 and suggest that low affinity of interaction of CGNL1 with ZO-1, and CGNL1 dual localization at the TJ and ZA, are responsible for the lack of effect of CGNL1 KO on ZO-1 accumulation at TJs.

CGN promotes the extended conformation of ZO-1 in cells

ZO-1 undergoes heterodimerization and tension-dependent folding and stretching/extension (24). In stretched/extended ZO-1, the N and C terminus of ZO-1 are detected as spatially separated by structured illumination microscopy (SIM), whereas in folded ZO-1, their signals spatially overlap (24). Under normal conditions in confluent epithelial cells, junction-associated ZO-1 is extended and sequesters the transcription factor DbpA at TJs (24). ZO-2 binding to ZO-1 at TJs promotes the extended state even when actomyosin contractility is reduced. However, when cells are depleted of ZO-2 and the integrity and contractility of the actomyosin cytoskeleton is disrupted, for example, by treatment with the myosin inhibitor blebbistatin, junctional ZO-1 becomes folded and does not recruit DbpA to junctions (24). Thus, junctional DbpA is an indicator of extended ZO-1 in cultured cells. We have proposed that the ZU5 domain contributes to intramolecular interactions that stabilize the folded conformation (24), and therefore we hypothesized that CGN binding to ZU5 could block ZU5-dependent intramolecular interactions and promote the ZO-1 extended conformation. To test this hypothesis, we overexpressed a small N-terminal fragment of CGN, that contains the ZIM motif (GFP-CGN(1-70)), in Eph4 cells and assessed junctional DbpA pools. As we have shown previously (24), ZO-1 retained DbpA at junctions in ZO-2-depleted cells (*arrows* in Fig. 6*A*, *cyan panels*). In addition, when expressed in these cells, the CGN ZIM-containing construct was localized junctionally, consistent with its binding to ZO-1 (*arrow*, Fig. 6*A*, *bottom green panel*), and its expression did not affect DbpA labeling. In contrast, as shown previously, DbpA junctional localization was undetectable in

cells depleted of ZO-2 and treated with blebbistatin (*arrowhead*, Fig. 6*B*, *upper cyan panel*) (24). Importantly, overexpression of the CGN ZIM construct (GFP-CGN(1-70)) in these cells rescued the junctional localization of DbpA (*arrow* in Fig. 6*B*, *bottom cyan panel*), consistent with the extended conformation of ZO-1. To further confirm the role of CGN in the extended conformation of ZO-1, we used CGN-KO Eph4 cells. Depletion of ZO-2 in these cells resulted in decreased labeling for DbpA at junctions (*arrowhead* in Fig. 6*C*, *bottom green panel*), indicating that loss of CGN phenocopies treatment of ZO-2-depleted cells with blebbistatin.

Next, we used SIM to evaluate the role of the ZU5 domain, and hence ZO-1 interaction with CGN, in the conformation of ZO-1. ZO-1 tagged with N-terminal myc and C-terminal hemagglutinin (HA) tags was expressed in the background of Eph4 ZO-1-KO cells, and cells were labeled with anti-myc and anti-HA antibodies, to detect the N and C termini of ZO-1 (24), and were depleted of ZO-2 with or without blebbistatin (IB analysis in Fig. 6*D*). As shown previously, the tags were detected as spatially separated when FL ZO-1 was expressed in cells treated either with si-Control or with depletion of ZO-2 without blebbistatin (*green/red arrows* in Fig. 6, *E* and *F*, alignment of beads in Fig. 6*J*, signal/distance profile in Fig. 6*K*). In contrast, the tags were overlapped when cells were depleted of ZO-2 and simultaneously treated with blebbistatin, indicating the folded conformation (*yellow arrow* in Fig. 6*G*, signal/distance profile in Fig. 6*K*) (24). When a construct of ZO-1 lacking the ZU5 domain was expressed (myc-ZO-1-ΔZU5-HA), the ends of ZO-1 were overlapped in both the presence (*yellow arrow*, Fig. 6*H*, signal/distance profile in Fig. 6*K*) and the absence (*yellow arrow*, Fig. 6*I*, signal/distance profile in Fig. 6*K*) of ZO-2, without treatment with blebbistatin. Thus, the lack of the ZU5 domain promotes the folded conformation of ZO-1.

CGN promotes the extended conformation of ZO-1 in vitro

GST-DbpA interacts with the isolated ZPSG region of ZO-1 by pull-down assay, but not with FL ZO-1 (32), suggesting that purified recombinant FL ZO-1 in solution is in a folded conformation (24). Heterodimerization with ZO-2 promotes the interaction of ZO-1 with DbpA *in vitro*, suggesting that this heterodimerization promotes the extended ZO-1 conformation by interfering with intramolecular ZO-1 interactions (24). In summary, in cells and *in vitro*, DbpA only binds to extended ZO-1, thus interaction with DbpA *in vitro* can be used as an assay for the conformational state of ZO-1. To test whether CGN unfolds ZO-1 *in vitro*, we used the previously established pull-down assay of binding of FL ZO-1 to GST-DbpA, in the presence of increasing amounts of either GFP or GFP-CGN(1–70) (Fig. 7, *A*–*C*). IB analysis showed that addition of sufficient amounts of GFP-CGN(1–70) resulted in detectable ZO-1 in GST-DbpA pulldowns, whereas addition of the same volumes of GFP-containing human embryonic kidney (HEK) lysate did not result in any detectable ZO-1 (Fig. 7, *A* and *B*, prey normalization in Fig. 7*C*). Moreover, the GST-DbpA-ZO-1 interaction was not an artifact because of binding of CGN(1–70) to DbpA, since the GFP-CGN(1–70) prey did not interact with GST-DbpA, which could instead still bind to its known interactor GEF-H1 (33), used as a positive control (Fig. 7*D*). Thus, since CGN(1–70) does not bind to DbpA, the rescue of junctional DbpA by CGN(1–70) (Fig. 6*B*) is not caused by its potential binding to DbpA but by the extended conformation of ZO-1.

We asked whether the ability of CGN to extend ZO-1 was due to a greater affinity of binding of CGN to the ZU5 domain, compared with the ZPSG1. To address this question, we measured the dissociation equilibrium constant (K_d) for the interaction of the CGN(1–70) sequence with ZU5, which was 40.4 nM (Fig. 7, *E*–*G*), whereas the calculated K_d for the ZPSG–ZU5 interaction is 66 nM (24). This suggests that CGN can promote the ZO-1 extended conformation by competitively binding to the ZU5 domain. Collectively, these experiments indicate that the interaction between the ZIM-containing region of CGN to the ZU5 domain of ZO-1 is required for CGN recruitment to junctions and promotes the extended conformation of ZO-1 and its binding to DbpA (Fig. 7*H*).

Discussion

Here, we investigated how CGN and CGNL1 regulate the TJ accumulation, dynamics, and conformation of ZO-1, a major protein involved in scaffolding of TJ transmembrane proteins, organization of the apical actomyosin cytoskeleton, and early embryo survival (34–38).

The ZU5 domain, a 110-residue domain at the C terminus of ZO-1 (39), was previously reported to promote efficient accumulation of ZO-1 at cell boundaries (40) and to interact with the Cdc42 effector kinase myotonic dystrophy kinase-related Cdc42-binding kinase β and with the Rho GEF ARHGEF11 (41–43). However, a role of these proteins in regulating ZO-1 accumulation at TJs was not described. Our results show that both CGN and CGNL1 bind to the ZU5 domain, albeit probably with quite different binding affinities, and that CGN is required to promote the efficient TJ accumulation not only of ZO-1, consistent with previous observations (44), but also of ZO-3. In contrast, CGNL1 does not affect the TJ assembly of either ZO-1 or ZO-3, and overexpression of CGNL1 does not rescue either ZO-1 or ZO-3 at junctions of double-KO cells, suggesting that CGNL1 binds too weakly to the ZU5 domain of ZO-1 to regulate its TJ assembly. A construct of ZO-1 lacking the ZU5 domain shows reduced accumulation at TJs, suggesting that CGN plays a key role in regulating TJ assembly of ZO-1. The mechanisms that regulate the TJ assembly of ZO-3 are poorly understood. Although ZO-3 can heterodimerize with ZO-1 (45), the observation that overexpression of ZO-1 did not rescue the decreased junctional accumulation of ZO-3 in CGN-KO cells suggests that CGN does not control ZO-3 accumulation at TJs through ZO-1. In addition, although we identified an interaction of the C-terminal region of ZO-3 with CGN, the role of this region in ZO-3 dynamics and conformation is not known. Thus, future studies should investigate the basis for ZO-3 assembly at TJs, its potential mechanoregulation, and the mechanisms through which CGN regulates ZO-3 accumulation at TJs.

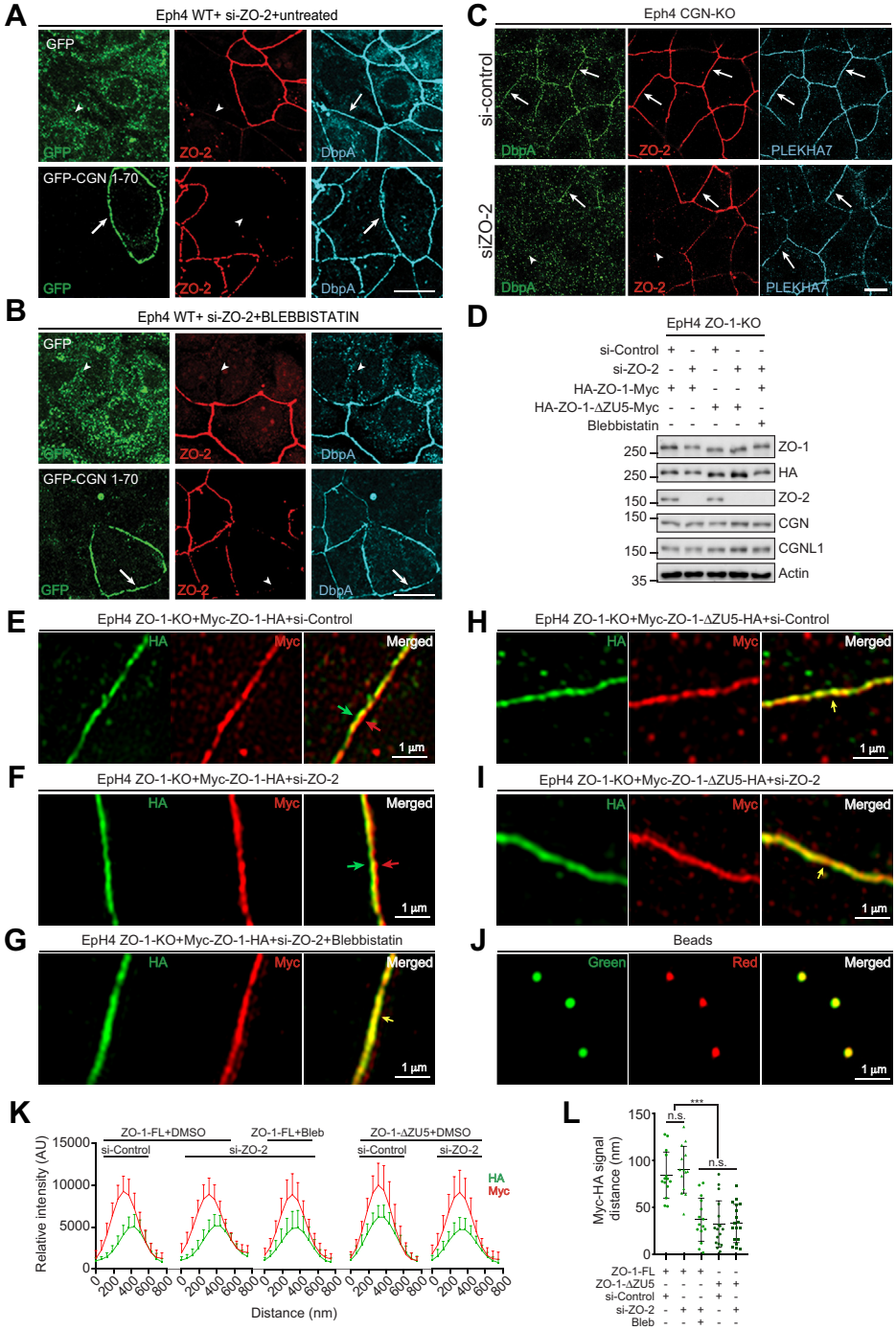

Figure 6. The ZU5–cingulin interaction promotes the extended conformation of ZO-1 in cells. *A* and *B*, IF microscopy analysis of the junctional localization of DbpA (*cyan*) in WT Eph4 cells depleted of ZO-2 and overexpressing either GFP (*top panels*) or GFP-CGN(1–70) (*bottom panels*) (*green*) either untreated (*A*) or treated with blebbistatin (*B*). ZO-2-depleted cells are identifiable as lacking ZO-2 (*red*) labeling (*arrowheads*). *C*, IF analysis of the junctional localization of DbpA (*cyan*) in CGN-KO Eph4 cells either treated with control-siRNA (si-control, *top*) or depleted of ZO-2 (siZO-2, *bottom*). *A–C*, PLEKHA7 (*cyan*) was used as a junctional marker. *Arrows* and *arrowheads* indicate normal and reduced/undetected junctional staining, respectively. The scale bars represent 10 µm. *D–L*, analysis of ZO-1 conformation by SIM. *D*, IB analysis of lysates of Eph4-ZO-1-KO cells used for SIM imaging (*E–I*), with the indicated antibodies. *E–I*, SIM images of ZO-1-KO Eph4 cells expressing either exogenous myc-ZO-1-HA full-length (*E–G*) or exogenous myc-ZO-1-ΔZU5-HA (*H–I*) and either treated with si-Control and DMSO (*E* and *H*), or treated with si-ZO-2 and DMSO (*F* and *I*), or treated with si-ZO-2 and blebbistatin (*G*). *Red* (Cy3) and *green* (Alexa 488) fluorophores (*insets/arrows*) label N-terminal and C-terminal ends of ZO-1. *Yellow arrows* indicate overlapped signal. *E* and *F*, show unfolded conformation (shift between *red* and *green*). *G*, shows control for folded conformation (overlap between *red* and *green*). *J*, multicolor bead alignment (to exclude that shift is due to spherical aberrations). *K*, distribution of fluorophores/tag signal intensities as a function of distance between intensity peaks. *L*, calculated distance between intensity peaks in the indicated experimental conditions (*E–I*). Error bars (*K* and *L*) indicates SD (n = 14–18).

We provide evidence that CGN binding to the ZU5 domain promotes the extended conformation of ZO-1. Junctional DbpA labeling is an established assay to detect the extended conformation of ZO-1, and we showed previously that both depletion of ZO-2 and simultaneous disruption of the acto-myosin cytoskeleton, for example by treatment with

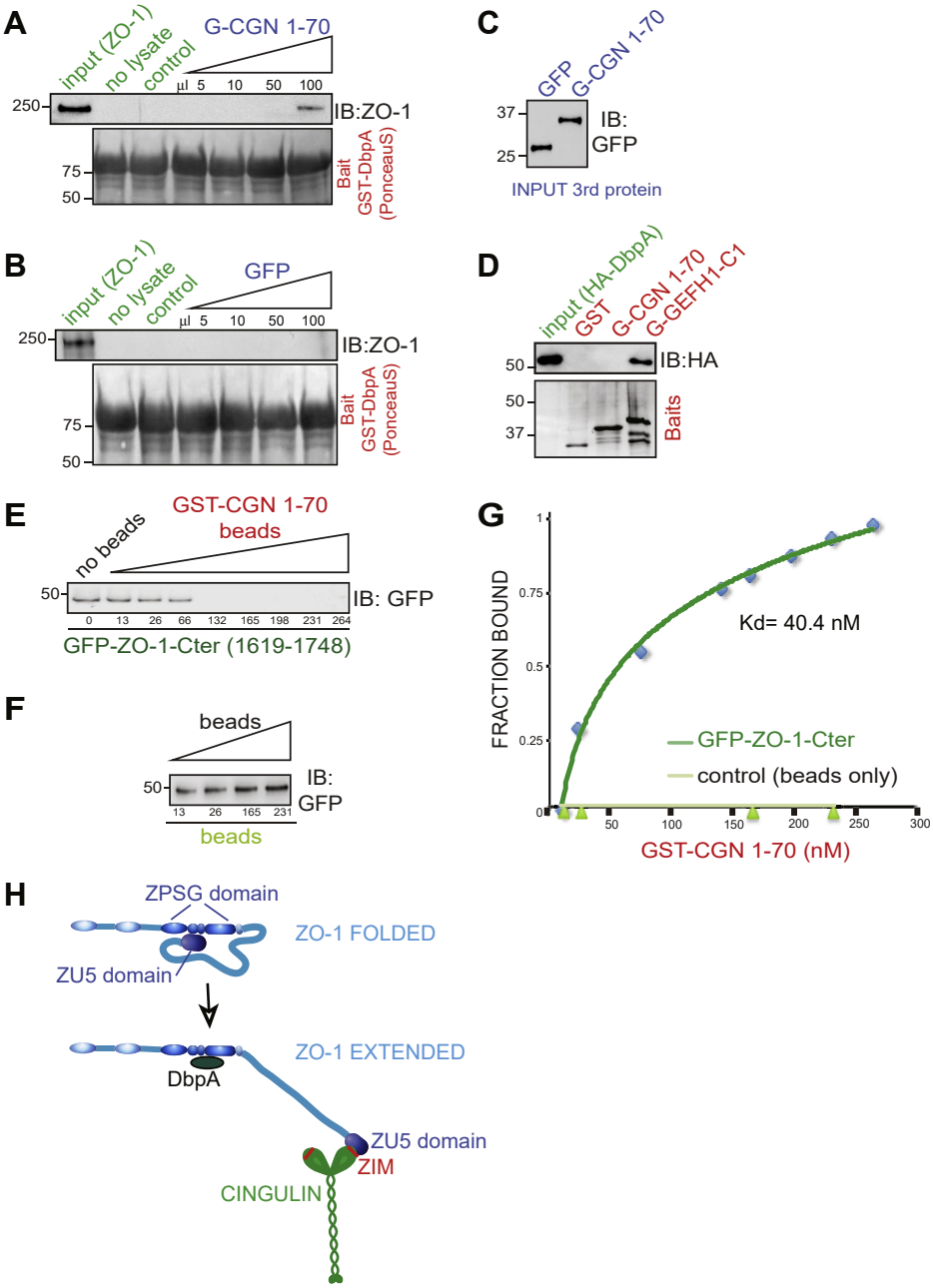

Figure 7. Cingulin (CGN) binding to the ZU5 domain extends ZO-1. *A* and *B*, IB analysis, using anti-ZO-1 antibodies, of full-length ZO-1 prey (from baculovirus-infected insect cells) in GST pulldowns using GST-DbpA as a bait and increasing amounts of either GFP-CGN(1–70) (*A*) or GFP (*B*, negative control) as third protein. Note that HEK cell lysates contain undetectable amounts of endogenous ZO-1 ("control" lane). *C*, IB analysis of normalization of third added protein (either GFP or GFP-CGN(1–70), with anti-GFP antibodies). *D*, IB analysis of HA-DbpA prey in GST pulldowns using GST-CGN(1–70) and GST-GEF-H1 as baits. *E–G*, measurement of the affinity of interaction between CGN(1–70) and Cter/ZU5. *E*, IB analysis of supernatant depletion assay. Depletion is achieved by adding increasing amounts of GST-CGN(1–70)-coated beads to the supernatant containing prey protein. Supernatant depletion by beads alone (control) is shown in (*F*). Numbers below each lane (*K–I*) indicate concentration (nanomolar) of recombinant bait protein used to deplete supernatant. *G*, plots of equilibrium binding isotherms, where fraction of prey protein bound (total minus remaining) is plotted against the concentration of the GST-CGN(1–70) used for depletion (24). *H*, scheme showing conformational change of ZO-1 from folded to extended, and consequent interaction of DbpA with the ZPSG domain of ZO-1, following binding of CGN to the ZU5 domain.

blebbistatin, are required to promote ZO-1 extended conformation in WT cells (24). Here we show, first, that overexpression of the ZO-1-binding fragment of CGN rescued junctional DbpA in ZO-2-depleted cells treated with blebbistatin. Second, KO of CGN was sufficient to abolish junctional DbpA localization in cells depleted of ZO-2, without blebbistatin treatment. Third, the ZO-1-binding N-terminal fragment of CGN was sufficient to promote the ZO-1-extended conformation *in vitro*, based on its interaction with DbpA in GST pulldowns. Fourth, SIM of exogenous ZO-1 with N-terminal and C-terminal tags showed that ZO-1 lacking the ZU5 domain is in a folded conformation under conditions in which FL ZO-1 is extended. Since the ZO-1 construct lacking the ZU5 domain is detectable laterally when exogenously

expressed, we speculate that this lateral pool of ZO-1 is imaged by SIM as folded in cells containing ZO-2. Concerning the mechanisms through which CGN promotes the extended conformation of ZO-1, we proposed that the folded conformation of ZO-1 is stabilized by the ZPSG–ZU5 interaction (24), and we show here that CGN binds to the ZU5 domain. Thus, our results suggest that CGN could promote the extended conformation of ZO-1 by competitively disrupting the ZU5–ZPSG1 interaction. Moreover, since the KO of CGN phenocopies treatment with blebbistatin in ZO-2-depleted cells, an additional mechanism through which CGN could extend ZO-1 is by linking ZO-1 to the actomyosin cytoskeleton through an interaction with myosin (14, 46). This hypothesis is currently being tested. In summary, our studies indicate the existence of a positive feedback loop, whereby CGN requires ZO-1 to be recruited to TJs, and in turn it promotes the ZO-1-extended conformation and stabilization at TJs.

The conformation of ZO-1 is mechanistically important for TJ assembly, since the ZO-1-extended conformation is required for its liquid–liquid phase separation and subsequent TJ assembly (25). However, the extended conformation of ZO-1 occurs in cytoplasmic condensates independently of junctional localization, and DbpA is found within condensates of purified ZO-1 *in vitro* (25), suggesting that multivalent interactions can promote ZO-1-extended conformation independently of junction-associated actomyosin-dependent stretching. Thus, the observation that the KO of CGN did not result in a complete loss of junctional ZO-1 suggests that redundant CGN-independent mechanisms, which likely include heterodimerization with other ZO proteins (24), interaction with actomyosin-binding AJ-associated proteins, such as α-catenin and vinculin (47), increased mechanical tension at AJ (28), and regulation by phosphorylation (25) contribute to the extended conformation and TJ assembly of ZO-1. Importantly, we show that ZO-1 lacking the ZU5 domain (ZO-1-ΔZU5) has markedly higher mobility and decreased junctional accumulation compared with FL ZO-1, increased localization along lateral contacts, and a folded conformation when expressed in the context of ZO-1-KO cells, as determined by SIM. Interestingly, endogenous Venus-tagged ZO-1 is detectable along lateral contacts of live cells, at concentrations below those required for liquid–liquid phase separation (25), but endogenous ZO-1 cannot be detected laterally by IF on fixed cells. Together, these observations suggest that lateral ZO-1 is in a folded conformation, and ZU5-mediated interactions contribute to triggering the extended conformation of ZO-1 at junctions. Thus, we propose that the dynamic equilibrium between cytoplasmic, junction-associated (phase-separated), and lateral contact–associated (non–phase-separated) ZO-1 is fine-tuned, among other mechanisms, by the ZU5-mediated interaction with CGN. Since CGN is localized apically during the biogenesis of TJs in *Xenopus* embryos (22, 48), our results also suggest that CGN contributes to the apical recruitment and stabilization of the TJ-associated pool of ZO-1 through its binding to the ZU5 domain.

In conclusion, our results show that the ZU5 domain of ZO-1 interacts with the ZIM sequences of CGN and CGNL1 and that CGN promotes the accumulation of ZO-1 and ZO-3 at TJs, and the stabilization, slower dynamics, and extended conformation of ZO-1. These results advance our knowledge on the molecular mechanisms underlying the regulation of ZO-1 and of the architecture and dynamic assembly of TJs.

Experimental procedures

Experimental model and subject details

Eph4 (mouse mammary epithelial cell line) WT and ZO-1-KO (a gift from the Tsukita laboratory, Osaka University) cells, MDCK II (a gift from A. Fanning, Anderson laboratory, University of North Carolina), mCCD (a gift from the Feraille laboratory, University of Geneva), and HEK293T cells were cultured at 37 °C, 5% CO_2 in Dulbecco's Modified Eagle's Medium (DMEM) containing 10% or 20% fetal bovine serum (FBS) (for mCCD). For Eph4, MDCK and mCCD culture media were supplemented with 1% nonessential amino acids, 100 units/ml penicillin, and 100 μg/ml streptomycin (24, 31, 49). MDCK lines stably transfected with eGFP-hZO-1 constructs (for IF and FRAP microscopy) were maintained in DMEM 1 g/l glucose supplemented with 10% FBS, 15 mM Hepes, and 50 ng/ml doxycycline.

Cell lines KO for either CGN or CGNL1 or both were generated using CRISPR–Cas9 gene editing technology, designing guide RNA using the Zhang Lab CRISPR design tool, targeting exons that are present in all major transcripts of *CGN* and *CGNL1*. For mouse *CGN* and *CGNL1* (m*CGN*, m*CGNL1*), to generate Eph4 and mCCD KO lines, the target sequences for the CRISPR–Cas9 were selected in exon 2 (Table S1). For canine *CGN* and *CGNL1* (c*CGN*, c*CGNL1*), to generate MDCK KO lines, the target sequences were selected in exon 1 (Table S1). The guide RNAs were subcloned into the BbsI site of pSpCas9(BB)-2A-GFP (PX458) CRISPR plasmid. Cells were transfected using Lipofectamine 2000. At 48 h post-transfection, single cells were sorted (using a Beckman Coulter MoFlo Astrios sorter; Flow Cytometry Service, University of Geneva Medical School) into 96-well tissue culture plates. Single clones were further amplified and screened for the KO using IB and IF microscopy analyses, based on which two to three CGN-KO and CGNL1-KO clones (one CGNL1-KO clone for Eph4) were selected and verified by sequencing. For sequencing, genomic DNA was extracted using DNeasy Blood & Tissue kit, the genomic loci of *CGN* and *CGNL1* (around 500 bp upstream and 600 downstream of target sequence) were amplified by PCR using specific primers (Table S1), and subcloned into pBluescript II KS(+) using restriction enzymes SacII and XhoI for m*CGN*, XbaI, and EcoRI for m*CGNL1* and c*CGN* and BamHI and SalI for c*CGNL1*. The T7 primer was used for sequencing inserts for genotyping.

To generate CGN/CGNL1 double-KO MDCK clones, CGN-KO (to generate clone 21D3) or CGNL1-KO (to generate clone 11C9) clones were transfected with aforementioned CGNL1-KO or CGN-KO CRISPR–Cas9 constructs,

respectively, sorted by FACS, and screened as described previously for single KO.

Immunofluorescence labeling and microscopy

Antibodies for IF microscopy are described in Table S1.

Cells were cultured either on glass coverslips in 24-well plates for 3 days seeded at a density of 1 to 2 × 10^5 cells/well or on 6-well (24-mm) Transwell filters (pore size of 0.4 μm, polyester) for 5 days seeded at a density of 5 × 10^5 cells (cells on Transwells shown in Figs. 5, S2, *E* and *L*, and S4, *A* and *C*). For analysis of protein localization in cells expressing exogenous constructs, cells were typically transfected 24 h after seeding, using Lipofectamine2000 and 1 μg of DNA, when applicable treated 48 h later with drugs (either DMSO or blebbistatin 50 μM for 16 h), and fixed for IF 4 days after seeding. IF for cells grown on coverslips was carried out by washing cells 2× with cold PBS, fixing in methanol at −20° for 10 min, washing 3 × 5 min with PBS, incubating with primary antibody (either at room temperature [RT] for 1 h or for 16 h at 4 °C), followed by washing 3× with PBS, incubating with secondary antibody (30 min at 37 °C in a humidified chamber), washing 3× with PBS, and mounting either with Vectashield with 4′,6-diamidino-2-phenylindole or Fluoromount-G. For IF localization of DbpA, we used the method previously described (32). Briefly, cells were permeabilized with actin stabilization buffer (100 mM KCl, 3 mM $MgCl_2$, 1 mM $CaCl_2$, 200 mM sucrose, 10 mM Hepes, pH 7.1 containing 0.1% Triton X-100) for 1 min at RT, fixed with ice-cold methanol for 7 min at −20 °C, followed by ice-cold acetone for 30 s at RT. Cells were then blocked with blocking buffer (PBS containing 0.5% bovine serum albumin [BSA] and either 10 mM glycine or 0.3% gelatin) for 30 min at RT, before incubation with antibodies. Slides were imaged either on a Zeiss LSM800 confocal microscope using a Plan-Apochromat 63×/1.40 oil objective at a resolution of 1024 × 1024px or on an upright microscope Leica DM4B using 63× oil objective at a resolution of 2048 × 2048px (pixel size = 0.10 μm). Images were extracted from.-lif,.lsm or.czi files using Fiji/ImageJ (NIH, Open Source, https://fiji.sc), adjusted and cropped using Adobe Photoshop, and placed into Adobe Illustrator documents for figure preparation.

For Z-stack analysis (Fig. 4, *A*–*C*), MDCK II cells were stably transfected with eGFP-hZO-1 or eGFP-hZO-1ΔZU5 and grown on 6-well (24 mm) polyester Transwell inserts with a pore size of 3.0 μm (Corning) for 7 days in DMEM 1 g/l glucose supplemented with 10% FBS, 15 mM Hepes, and 40 ng/ml doxycycline. Transwells were washed in ice-cold PBS, fixed in 2% paraformaldehyde for 20 min at RT, washed with IMF buffer (0.1% Triton X-100, 0.15 M NaCl, 5 mM EDTA, 20 mM Hepes, pH 7.5, and NaN_3). Transwells were blocked in 3% BSA in IMF buffer and stained overnight with 1/1000 rat anti-E-cadherin (Thermo Fisher) followed by 1/2000 Rhodamine-RedX anti-rat (Jackson Laboratory) and mounted with Prolong Diamond antifade. A Nikon A1Rsi laser scanning confocal microscope was used to collect 512 × 512px z-stack images in 0.2 μm steps with 4× line scanning in resonant mode with a Plan Apo λ 60× oil objective. ZO-1 and E-cadherin signal were imaged with the 488 (eGFP) and 561 laser lines, respectively. Image acquisition parameters were constant for each target across the cell lines. Z-stack images were post-processed with the Nikon NIS Elements denoise algorithm, and maximum intensity and xz orthogonal projections are presented.

Structured illumination microscopy

SIM microscopy and image acquisition, reconstruction, and processing were carried out as described (24), except that Eph4 ZO-1-KO cells were transfected with either myc-ZO-1-HA (FL) or with myc-ZO-1-ΔZU5-HA. Following treatment either with DMSO or blebbistatin, cells were fixed with cold methanol and double stained with antibodies against myc and HA, followed by Cy-3 and Alexa488-labeled secondary antibodies. The Plot-Profile plugin of ImageJ was used to plot pixel intensities (*y*-axis) of red and green fluorophores as a function of distance (*x*-axis) across the junction. The *x*-coordinate of the maximum intensity peak was determined using the Prism software (mean function of the Gaussian curve).

Measurement of cell proliferation

To measure cell proliferation, cells were plated in 12-well plate (75,000 cells/well) and trypsinized and counted in a hemocytometer each day, for 6 days.

Plasmids

Constructs of GFP-tagged fragments of ZO-1 in pCDNA3.1(+) (24), ZO-1 for expression in insect cells (24), HA-DbpA in pCDNA3.1(+) (32), GFP-myc-his in pCDNA3.1(−) (50), cyan fluorescent protein-HA in pCDNA3.1(+) (32), and GFP-myc in pTRE2Hyg (51) were described previously.

The following new constructs (see also Table S1) were generated by PCR amplification with appropriate oligonucleotides and subcloned into the indicated cloning site (m = mouse, h = human, c = canis). GFP-hZO-1 (1698–1748 amino acids) (S1874) and GFP-hZO-1 (1550–1650 amino acids) (S1875) were cloned into NotI–KpnI sites of pCDNA3.1(+). The FL myc-hZO-1-HA (1–1748) (S1947) and the mutant lacking ZU5 domain myc-hZO-1-ΔZU5-HA (1–1619 amino acids) (S2161) were cloned into BamH1–XhoI sites of pCDNA3.1(+). The FL mCGN-myc-his (1–1192 amino acids) (S2407) and the mutant lacking ZIM domain mCGN-ΔZIM-myc-his (71–1192 amino acids) (S2408) were cloned into XhoI–KpnI sites of pcDNA3.1(−). GFP-hCGN (1–1203 amino acids) (S2508) and the mutant lacking ZIM domain (GFP-hCGN-ΔZIM) (71–1203 amino acids) (S2509) were cloned into NotI-Acc65I of pCDNA3.1(−). hCGN-HA (1–1203 amino acids) (S2411) was cloned into BamHI–XbaI sites of pCDNA3.1(+). hCGNL1-HA (1–1302 amino acids) (S2442) and mutant lacking ZIM domain (hCGNL1-HA-ΔZIM) (81–1302 amino acids) (S2510) were cloned into

BamHI–NotI sites of pCDNA3.1. To generate FL eGFP-tagged human ZO-1 for FRAP analysis (eGFP-hZO-1), the eGFP-hZO-1 gene (5.274 bp) was digested from pEF1-eGFP ZO-1 (38) with Kpn1 and inserted into the Kpn1 site of pPBH-TREtight-eGFP-C (Systems Biosciences). eGFP-hZO-1-ΔZU5 was designed by PCR-based site-directed mutagenesis on EGFP-ZO-1, introducing a stop codon and MIuI restriction site at the beginning of the C-terminal ZU5 domain, using the QuikChange Lightning site-directed mutagenesis kit. The resulting eGFP-hZO-1ΔZU5 corresponds to residues 1 to 1620 of FL hZO-1.

GST-DbpA and GST-GEF-H1 were gifts from the Matter-Balda laboratory. New GST-tagged constructs were generated by PCR and subcloning in the sites indicated sites in parentheses. cCGN (1–70 amino acids) (S1851) (EcoRI–NotI) comprises the ZIM region (29). GST-tagged hZO-1-Cter (1523–1748, sequence corresponding to residues 1447–1692 of ZO-1 variant-4, isoform d) (S1789) (EcoRI–XhoI) comprises the complete hZU5 domain (1634–1748). GST-tagged mZO-1-CterLarge (1520–1745) (S2511) (BamHI–NotI) comprises the complete mZU5 domain (1631–1745) and upstream sequence, since fusion proteins comprising exclusively the ZU5 domain (either human or mouse) were not stable. The GST-cZO-3(Cter) (450–832) construct (S1986) (BamHI–NotI) comprises the PDZ3, SH3, and GUK domains of ZO-3. All new plasmids were verified by sequencing.

Recombinant protein expression, GST pulldown, and supernatant depletion assays

GST fusion proteins were expressed in BL21 bacteria and purified by affinity chromatography on either Glutathione Sepharose (32) or magnetic beads. Pulldowns were carried out using lysates either from insect cells expressing FL ZO-1 or from lysates of HEK293T cells expressing either GFP-tagged ZO-1 fragments, GFP-tagged CGN constructs, or HA-tagged DbpA and CGNL1 constructs (preys) as previously described (49, 52), after normalization of preys and baits.

To determine the K_d of interaction between the ZU5 domain of ZO-1 (1619–1748 = Cter) and the CGN1-70 fusion protein, we used a quantitative GST-pulldown "Supernatant Depletion Assay" (24). Increasing volumes (1, 2, 5, 10, 12.5, 15, 17.5, and 20 μl) of Glutathione Sepharose beads preloaded with GST-CGN(1–70) bait (0.666 μM) were added to prey protein (GFP-hZO-1-Cter), in a total volume of 0.5 ml co-IP buffer (150 mM NaCl, 20 mM Tris–HCl, pH 7.5, 1% Nonidet P-40, 1 mM EDTA, and complete protease inhibitor). As a negative control, beads preincubated with co-IP buffer alone (1, 2, 5, and 10 μl) were added to the prey. After 16 h incubation at 4 °C, beads were pelleted at 16,000*g*, and the prey proteins remaining in the supernatant were analyzed by SDS-PAGE and immunoblotting. GST pull-down experiments to assess the effect of CGN(1–70) on the interaction between DbpA and FL ZO-1 were carried out by incubating GST-DbpA (5 μg) with insect cell lysate containing FL ZO-1, in the presence of increasing volumes of normalized HEK293T cell lysates containing either GFP-CGN(1–70) or GFP, this latter as a negative control. Although it is unlikely that sufficient concentrations of additional interacting partners of baits and preys are present in the GST pull-down assays and might influence some of the results, this possibility cannot be formally excluded. Concentration of recombinant proteins was determined by densitometric analysis of Coomassie-stained SDS gels, compared with a BSA standard curve.

Transfection, siRNA-mediated ZO-2 depletion, and exogenous expression of proteins

For transfections for rescue experiments, cells plated on glass round 12 mm coverslips in 24-well plate (100,000 cells/well) were transfected the next day using Lipofectamine 2000 or jetOPTIMUS DNA transfection reagent and fixed for IF 72 h post-transfection.

For siRNA-mediated ZO-2 depletion (target sequence in Table S1), cells were transfected with Lipofectamine RNAiMAX 24 h after plating, using siRNA negative control. For siRNA and DNA cotransfections, Eph4 cells were transfected 1 day after plating with the mix of siRNA and DNA using Lipofectamine 2000, 48 h post-transfection cells were treated with 50 μM blebbistatin for 16 h and then fixed (24).

For FRAP experiments, MDCK II cells were cotransfected with pPBH-TREtight-eGFP-hZO-1 constructs and pSPB-transposase using Lipofectamine and selected in low-glucose DMEM containing hygromycin B medium to produce stabling expressing EGFP-hZO-1 or EGFP-hZO-1ΔZU5 cell lines.

For prey production, HEK293T cells were plated in 10 cm dishes (2×10^6 cells/dish), transfected the next day using Lipofectamine 2000, and lysates were prepared 48 h post-transfection.

Overexpression of ZO-1 for condensate analysis

To study recruitment of CGN and CGNL1 client proteins by ZO-1 condensates, 1×10^5 MDCK II cells were seeded onto glass coverslips placed in 24-well plates. About 24 h after plating, cells were transfected with 1.5 μg of ZO-1 DNA construct(s) per dish, using jetOPTIMUS. About 48 h post-transfection, cells were fixed, labeled, and observed by IF microscopy.

Fluorescence recovery after photobleaching

MDCK II cells stably expressing EGFP-hZO-1 or EGFP-hZO-1ΔZU5 were seeded at confluence on collagen-coated glass 35 mm dishes (MatTek) and induced with 40 ng/ml doxycycline in low-glucose DMEM supplemented with 10% FBS and 15 mM Hepes for 72 h prior to analysis. FRAP assays were conducted in Hanks' balanced salt solution in a temperature-controlled stage on a Nikon A1R laser scanning confocal microscope using a 60× objective. Cell junctions were photobleached for 5 s at 30% 488 nm laser power, and images were acquired at regular intervals for a recovery period of 7 min. For kymographs (Fig. 4*G*), the time scale was from pre-bleach (0) up to 420 s. The first 2 min post-bleach

images were acquired every 2 s, and the last 5 min of acquisition images were acquired every 5 s. Background fluorescence was subtracted from raw data, and mobile fraction and $t_{1/2}$ were calculated by fitting to an exponential curve (23).

For videos (125 frames), MP4 files were created from ND2 files using NIS elements software (Laboratory Imaging s.r.o for Nikon Corporation). Each frame is 200 ms, and the compression settings were H.264 high quality. The first five are pre-bleach acquired at 2 s intervals, the next 60 are immediately following bleaching at 2 s intervals, and the remaining 60 frames were acquired at 5 s intervals.

Immunoblotting

Cell lysates were obtained using radioimmunoprecipitation assay buffer (RIPA: NaCl 150 mM, Tris-HCl 40 mM, pH 7.5, EDTA 2 mM, glycerol 10%, Triton X-100 1%, sodium deoxycholate 0.5%, SDS 0.2%) containing either 1× cOmplete (Roche) or Pierce protease inhibitor cocktails, and immunoblotting was performed as previously described (24, 31). β-tubulin was used for protein loading normalization in immunoblots. Numbers on the left of immunoblots indicate migration of molecular size markers (kilodalton).

Quantification and statistical analysis

Data processing and analysis were performed using GraphPad Prism. All experiments were carried out at least three times, when applicable on multiple clonal lines. Statistical significance of quantitative data was determined by either unpaired two-tailed Student's t test (when comparing two sets of data) or ordinary one-way or two-way ANOVA with Tukey's post hoc test (for multiple comparisons), (ns = not significant difference $p > 0.5$, significant $^{*}p \le 0.05$, $^{**}p \le 0.01$, $^{***}p \le 0.001$, and **** $p \le 0.0001$). For statistical analysis of FRAP data, outliers were identified using the ROUT method (Q = 1%), and significance was determined using the unpaired t test ($^{****}p \le 0.0001$).

Analysis of immunofluorescence microscopy data

For the quantification of junctional immunofluorescent microscopy signal, pixel intensity for each channel was measured in the selected junctional area using the polyhedral tool of Fiji/ImageJ, and the averaged background signal of the image was subtracted. Relative intensity signal was expressed as a ratio between the signal of protein of interest and an internal junctional reference (either PLEKHA7, or occludin, or PLEKHA6 or E-cadherin). Between 10 and 45 junctional segments of each phenotype were analyzed for each experiment.

Analysis of immunoblotting data

For the quantification of IB signals, densitometric analysis was carried out on data from at least three separate experiments. Each time the signal was normalized to tubulin, used as reference for total protein loading, and expressed as percentage, taking the strongest signal as 100%.

Data availability

Data and materials are available from the corresponding author (S. C.), upon request.

Supporting information—This article contains supporting information (Table S1, Figs. S1–S5, and Movies S1 and S2) (11, 13, 24, 32, 33, 48–51, 53–57).

Acknowledgments—We thank all the colleagues cited in the text for their kind gift of cell lines and reagents, Thierry Laroche (EPFL, Lausanne, Switzerland) for assistance with SIM, Marine Mauperin for comments on the article, and the reviewers for their constructive comments.

Author contributions—S. C., D. S., E. V., F. R., and J. R. T. conceptualization; D. S., E. V., F. R., A. F., J. S., S. S., J. M. K., and S. C. methodology; E. V., F. R., D. S., J. M. K., and S. C. validation; D. S., E. V., F. R., I. M., L. J., and J. M. K. investigation; D. S., E. V., F. R., J. S., A. F., S. S., I. M., L. J., J. M. K., and S. C. resources; E. V., F. R., D. S., S. S., and J. M. K. data curation; S. C., E. V., D. S., F. R., and J. M. K. writing–original draft; S. C. writing–review & editing; E. V., D. S., F. R., S. S., and S. C. visualization; S. C. and J. R. T. supervision; S. C. project administration; S. C., J. R. T, and J. M. K. funding acquisition.

Funding and additional information—This study was supported by the Swiss National Fund for Scientific Research (N. 31003A_152899, N. 31003A_172809, N. 31003A_130520, and N.31003A_14997 [to S. C.]), by the National Institutes of Health (grants R01DK61931 and R01DK68271 [to J. R. T.]), and by the National Science Foundation (Major Research Instrumentation grant: no. 1229702 [to J. M. K.]). The content is solely the responsibility of the authors and does not necessarily represent the official views of the National Institutes of Health.

Conflict of interest—J. R. T. is a founder and shareholder of Thelium Therapeutics and has served as a consultant for Entrinsic, Immunic, and Kallyope. S. C. has served as a consultant for Immunic. All other authors declare that they have no conflicts of interest with the contents of this article.

Abbreviations—The abbreviations used are: AJ, adherens junction; BSA, bovine serum albumin; CGN, cingulin; CGNL1, paracingulin; DMEM, Dulbecco's modified Eagle's medium; eGFP, enhanced GFP; FBS, fetal bovine serum; FL, full length; FRAP, fluorescence recovery after photobleaching; GEF, guanine nucleotide exchange factor; GST, glutathione-*S*-transferase; HA, hemagglutinin; HEK, human embryonic kidney cell line; IB, immunoblot; IF, immunofluorescence; PLEKHA7, pleckstrin homology domain–containing family A member 7; mCCD, mouse cortical collecting duct epithelial cell line; MDCK, Madin–Darby canine kidney epithelial cell line; RT, room temperature; SIM, structured illumination microscopy; TJ, tight junction; ZA, *zonulae adhaerentes*; ZIM, ZO-1 interaction motif; ZO, *zonula occludens*.

References

1. Anderson, J. M., and Van Itallie, C. M. (2009) Physiology and function of the tight junction. *Cold Spring Harb. Perspect. Biol.* **1**, a002584
2. Otani, T., and Furuse, M. (2020) Tight junction structure and function revisited. *Trends Cell Biol.* **30**, 815–817

3. Tsukita, S., Tanaka, H., and Tamura, A. (2019) The claudins: From tight junctions to biological systems. *Trends Biochem. Sci.* **44**, 141–152
4. Stevenson, B. R., Siliciano, J. D., Mooseker, M. S., and Goodenough, D. A. (1986) Identification of ZO-1: A high molecular weight polypeptide associated with the tight junction (zonula occludens) in a variety of epithelia. *J. Cell Biol.* **103**, 755–766
5. Gumbiner, B., Lowenkopf, T., and Apatira, D. (1991) Identification of a 160 kDa polypeptide that binds to the tight junction protein ZO-1. *Proc. Natl. Acad. Sci. U. S. A.* **88**, 3460–3464
6. Balda, M. S., Gonzalez-Mariscal, L., Matter, K., Cereijdo, M., and Anderson, J. M. (1993) Assembly of the tight junction: The role of diacylglycerol. *J. Cell Biol.* **123**, 293–302
7. Zihni, C., Mills, C., Matter, K., and Balda, M. S. (2016) Tight junctions: From simple barriers to multifunctional molecular gates. *Nat. Rev. Mol. Cell Biol.* **17**, 564–580
8. Rouaud, F., Sluysmans, S., Flinois, A., Shah, J., Vasileva, E., and Citi, S. (2020) Scaffolding proteins of vertebrate apical junctions: Structure, functions and biophysics. *Biochim. Biophys. Acta Biomembr.* **1862**, 183399
9. Gonzalez-Mariscal, L., Betanzos, A., Nava, P., and Jaramillo, B. E. (2003) Tight junction proteins. *Prog. Biophys. Mol. Biol.* **81**, 1–44
10. Citi, S., Sabanay, H., Jakes, R., Geiger, B., and Kendrick-Jones, J. (1988) Cingulin, a new peripheral component of tight junctions. *Nature* **333**, 272–276
11. Umeda, K., Matsui, T., Nakayama, M., Furuse, K., Sasaki, H., Furuse, M., and Tsukita, S. (2004) Establishment and characterization of cultured epithelial cells lacking expression of ZO-1. *J. Biol. Chem.* **279**, 44785–44794
12. Ohnishi, H., Nakahara, T., Furuse, K., Sasaki, H., Tsukita, S., and Furuse, M. (2004) JACOP, a novel plaque protein localizing at the apical junctional complex with sequence similarity to cingulin. *J. Biol. Chem.* **279**, 46014–46022
13. Pulimeno, P., Paschoud, S., and Citi, S. (2011) A role for ZO-1 and PLEKHA7 in recruiting paracingulin to tight and adherens junctions of epithelial cells. *J. Biol. Chem.* **286**, 16743–16750
14. Cordenonsi, M., D'Atri, F., Hammar, E., Parry, D. A., Kendrick-Jones, J., Shore, D., and Citi, S. (1999) Cingulin contains globular and coiled-coil domains and interacts with ZO-1, ZO-2, ZO-3, and myosin. *J. Cell Biol.* **147**, 1569–1582
15. D'Atri, F., and Citi, S. (2001) Cingulin interacts with F-actin *in vitro*. *FEBS Lett.* **507**, 21–24
16. Paschoud, S., Guillemot, L., and Citi, S. (2012) Distinct domains of paracingulin are involved in its targeting to the actin cytoskeleton and regulation of apical junction assembly. *J. Biol. Chem.* **287**, 13159–13169
17. Yano, T., Torisawa, T., Oiwa, K., and Tsukita, S. (2018) AMPK-dependent phosphorylation of cingulin reversibly regulates its binding to actin filaments and microtubules. *Sci. Rep.* **8**, 15550
18. Mangan, A. J., Sietsema, D. V., Li, D., Moore, J. K., Citi, S., and Prekeris, R. (2016) Cingulin and actin mediate midbody-dependent apical lumen formation during polarization of epithelial cells. *Nat. Commun.* **7**, 12426
19. Vasileva, E., and Citi, S. (2018) The role of microtubules in the regulation of epithelial junctions. *Tissue barriers* **6**, 1539596
20. Citi, S., Pulimeno, P., and Paschoud, S. (2012) Cingulin, paracingulin, and PLEKHA7: Signaling and cytoskeletal adaptors at the apical junctional complex. *Ann. N. Y. Acad. Sci.* **1257**, 125–132
21. Van Itallie, C. M., Aponte, A., Tietgens, A. J., Gucek, M., Fredriksson, K., and Anderson, J. M. (2013) The N and C termini of ZO-1 are surrounded by distinct proteins and functional protein networks. *J. Biol. Chem.* **288**, 13775–13788
22. Fesenko, I., Kurth, T., Sheth, B., Fleming, T. P., Citi, S., and Hausen, P. (2000) Tight junction biogenesis in the early Xenopus embryo. *Mech. Dev.* **96**, 51–65
23. Shen, L., Weber, C. R., and Turner, J. R. (2008) The tight junction protein complex undergoes rapid and continuous molecular remodeling at steady state. *J. Cell Biol.* **181**, 683–695
24. Spadaro, D., Le, S., Laroche, T., Mean, I., Jond, L., Yan, J., and Citi, S. (2017) Tension-dependent stretching activates ZO-1 to control the junctional localization of its interactors. *Curr. Biol.* **27**, 3783–3795. e3788
25. Beutel, O., Maraspini, R., Pombo-Garcia, K., Martin-Lemaitre, C., and Honigmann, A. (2019) Phase separation of zonula occludens proteins drives formation of tight junctions. *Cell* **179**, 923–936.e911
26. Schwayer, C., Shamipour, S., Pranjic-Ferscha, K., Schauer, A., Balda, M., Tada, M., Matter, K., and Heisenberg, C. P. (2019) Mechanosensation of tight junctions depends on ZO-1 phase separation and Flow. *Cell* **179**, 937–952.e918
27. Yu, D., Marchiando, A., Weber, C., Raleigh, D., Wang, Y., Shen, L., and Turner, J. (2010) MLCK-dependent exchange and actin binding region-dependent anchoring of ZO-1 regulate tight junction barrier function. *Proc. Natl. Acad. Sci. U. S. A.* **107**, 8237–8241
28. Citi, S. (2020) Tight junctions as biomolecular condensates. *Curr. Biol.* **30**, R83–R86
29. D'Atri, F., Nadalutti, F., and Citi, S. (2002) Evidence for a functional interaction between cingulin and ZO-1 in cultured cells. *J. Biol. Chem.* **277**, 27757–27764
30. Wittchen, E. S., Haskins, J., and Stevenson, B. R. (1999) Protein interactions at the tight junction. Actin has multiple binding partners, and zo-1 forms independent complexes with zo-2 and zo-3. *J. Biol. Chem.* **274**, 35179–35185
31. Vasileva, E., Sluysmans, S., Bochaton-Piallat, M. L., and Citi, S. (2017) Cell-specific diversity in the expression and organization of cytoplasmic plaque proteins of apical junctions. *Ann. N. Y. Acad. Sci.* **1405**, 160–166
32. Spadaro, D., Tapia, R., Jond, L., Sudol, M., Fanning, A. S., and Citi, S. (2014) ZO proteins redundantly regulate the transcription factor DbpA/ZONAB. *J. Biol. Chem.* **289**, 22500–22511
33. Nie, M., Aijaz, S., Leefa Chong San, I. V., Balda, M. S., and Matter, K. (2009) The Y-box factor ZONAB/DbpA associates with GEF-H1/Lfc and mediates Rho-stimulated transcription. *EMBO Rep.* **10**, 1125–1131
34. Fanning, A. S., Jameson, B. J., Jesaitis, L. A., and Anderson, J. M. (1998) The tight junction protein ZO-1 establishes a link between the transmembrane protein occludin and the actin cytoskeleton. *J. Biol. Chem.* **273**, 29745–29753
35. Umeda, K., Ikenouchi, J., Katahira-Tayama, S., Furuse, K., Sasaki, H., Nakayama, M., Matsui, T., Tsukita, S., Furuse, M., and Tsukita, S. (2006) ZO-1 and ZO-2 independently determine where claudins are polymerized in tight-junction strand formation. *Cell* **126**, 741–754
36. Katsuno, T., Umeda, K., Matsui, T., Hata, M., Tamura, A., Itoh, M., Takeuchi, K., Fujimori, T., Nabeshima, Y. I., Noda, T., Tsukita, S., and Tsukita, S. (2008) Deficiency of zonula occludens-1 causes embryonic lethal phenotype associated with defected yolk sac angiogenesis and apoptosis of embryonic cells. *Mol. Biol. Cell* **19**, 2465–2475
37. Odenwald, M. A., Choi, W., Kuo, W. T., Singh, G., Sailer, A., Wang, Y., Shen, L., Fanning, A. S., and Turner, J. R. (2018) The scaffolding protein ZO-1 coordinates actomyosin and epithelial apical specializations *in vitro* and *in vivo*. *J. Biol. Chem.* **293**, 17317–17335
38. Van Itallie, C. M., Fanning, A. S., Bridges, A., and Anderson, J. M. (2009) ZO-1 stabilizes the tight junction solute barrier through coupling to the perijunctional cytoskeleton. *Mol. Biol. Cell* **20**, 3930–3940
39. Fanning, A. S., and Anderson, J. M. (2009) Zonula occludens-1 and -2 are cytosolic scaffolds that regulate the assembly of cellular junctions. *Ann. N. Y Acad. Sci.* **1165**, 113–120
40. McNeil, E., Capaldo, C. T., and Macara, I. G. (2006) Zonula occludens-1 function in the assembly of tight junctions in Madin-Darby canine kidney epithelial cells. *Mol. Biol. Cell* **17**, 1922–1932
41. Huo, L., Wen, W., Wang, R., Kam, C., Xia, J., Feng, W., and Zhang, M. (2011) Cdc42-dependent formation of the ZO-1/MRCKbeta complex at the leading edge controls cell migration. *EMBO J.* **30**, 665–678
42. Unbekandt, M., and Olson, M. F. (2014) The actin-myosin regulatory MRCK kinases: Regulation, biological functions and associations with human cancer. *J. Mol. Med. (Berl)* **92**, 217–225
43. Itoh, M., Tsukita, S., Yamazaki, Y., and Sugimoto, H. (2012) Rho GTP exchange factor ARHGEF11 regulates the integrity of epithelial junctions by connecting ZO-1 and RhoA-myosin II signaling. *Proc. Natl. Acad. Sci. U. S. A.* **109**, 9905–9910
44. Terry, S. J., Zihni, C., Elbediwy, A., Vitiello, E., Leefa Chong San, I. V., Balda, M. S., and Matter, K. (2011) Spatially restricted activation of RhoA

signalling at epithelial junctions by p114RhoGEF drives junction formation and morphogenesis. *Nat. Cell Biol.* **13**, 159–166
45. Wittchen, E. S., Haskins, J., and Stevenson, B. R. (2000) Exogenous expression of the amino-terminal half of the tight junction protein ZO-3 perturbs junctional complex assembly. *J. Cell Biol.* **151**, 825–836
46. [preprint] Vasileva, E., Rouaud, F., Spadaro, D., Huang, W., Colom, A., Flinois, A., Shah, J., Dugina, V., Chaponnier, C., Sluysmans, S., Mean, I., Jond, L., Roux, A., Yan, J., and Citi, S. (2020) Cingulin unfolds ZO-1 and organizes myosin-2B and g-actin to mechanoregulate apical and tight junction membranes. *BiorXiv*. https://doi.org/10.1101/2020.05.14.095364
47. Maiers, J. L., Peng, X., Fanning, A. S., and DeMali, K. A. (2013) ZO-1 recruitment to alpha-catenin–a novel mechanism for coupling the assembly of tight junctions to adherens junctions. *J. Cell Sci.* **126**, 3904–3915
48. Cardellini, P., Davanzo, G., and Citi, S. (1996) Tight junctions in early amphibian development: Detection of junctional cingulin from the 2-cell stage and its localization at the boundary of distinct membrane domains in dividing blastomeres in low calcium. *Dev. Dyn.* **207**, 104–113
49. Rouaud, F., Vasileva, E., Spadaro, D., Tsukita, S., and Citi, S. (2019) R40.76 binds to the alpha domain of ZO-1: Role of ZO-1 (alpha+) in epithelial differentiation and mechano-sensing. *Tissue barriers* **7**, e1653748
50. Guerrera, D., Shah, J., Vasileva, E., Sluysmans, S., Mean, I., Jond, L., Poser, I., Mann, M., Hyman, A. A., and Citi, S. (2016) PLEKHA7 recruits PDZD11 to adherens junctions to stabilize nectins. *J. Biol. Chem.* **291**, 11016–11029
51. Paschoud, S., Jond, L., Guerrera, D., and Citi, S. (2014) PLEKHA7 modulates epithelial tight junction barrier function. *Tissue barriers* **2**, e28755
52. Shah, J., Rouaud, F., Guerrera, D., Vasileva, E., Popov, L. M., Kelley, W. L., Rubinstein, E., Carette, J. E., Amieva, M. R., and Citi, S. (2018) A dock-and-lock mechanism clusters ADAM10 at cell-cell junctions to promote alpha-toxin cytotoxicity. *Cell Rep.* **25**, 2132–2147.e2137
53. Pulimeno, P., Bauer, C., Stutz, J., and Citi, S. (2010) PLEKHA7 is an adherens junction protein with a tissue distribution and subcellular localization distinct from ZO-1 and E-cadherin. *PLoS One* **5**, e12207
54. Sluysmans, S., Mean, I., Xiao, T., Boukhatemi, A., Ferreira, F., Jond, L., Mutero, A., Chang, C. J., and Citi, S. (2021) PLEKHA5, PLEKHA6 and PLEKHA7 bind to PDZD11 to target the Menkes ATPase ATP7A to the cell periphery and regulate copper homeostasis. *Mol. Biol. Cell* **32**, ar34
55. Balda, M. S., Garrett, M. D., and Matter, K. (2003) The ZO-1-associated Y-box factor ZONAB regulates epithelial cell proliferation and cell density. *J. Cell Biol.* **160**, 423–432
56. Fialka, I., Schwarz, H., Reichmann, E., Oft, M., Busslinger, M., and Beug, H. (1996) The estrogen-dependent c-JunER protein causes a reversible loss of mammary epithelial cell polarity involving a destabilization of adherens junctions. *J. Cell Biol.* **132**, 1115–1132
57. Wang, Y. B., Leroy, V., Maunsbach, A. B., Doucet, A., Hasler, U., Dizin, E., Ernandez, T., de Seigneux, S., Martin, P. Y., and Feraille, E. (2014) Sodium transport is modulated by p38 kinase-dependent cross-talk between ENaC and Na,K-ATPase in collecting duct principal cells. *J. Am. Soc. Nephrol.* **25**, 250–259